Maintenance of Interphase Chromosome Compaction and Homolog Pairing in *Drosophila* Is Regulated by the Condensin Cap-H2 and Its Partner Mrg15

Helen F. Smith,*,[1] Meredith A. Roberts,*,[1] Huy Q. Nguyen,†,[1] Maureen Peterson,†,[1] Tom A. Hartl,* Xiao-Jun Wang,* Joseph E. Klebba,‡ Gregory C. Rogers,‡ and Giovanni Bosco*,†,[2]

†Department of Genetics, Geisel School of Medicine at Dartmouth, Hanover, New Hampshire, 03755, *Department of Molecular and Cellular Biology and ‡Department of Cellular and Molecular Medicine University of Arizona, Tucson, Arizona, 85721

ABSTRACT Dynamic regulation of chromosome structure and organization is critical for fundamental cellular processes such as gene expression and chromosome segregation. Condensins are conserved chromosome-associated proteins that regulate a variety of chromosome dynamics, including axial shortening, lateral compaction, and homolog pairing. However, how the *in vivo* activities of condensins are regulated and how functional interactors target condensins to chromatin are not well understood. To better understand how *Drosophila melanogaster* condensin is regulated, we performed a yeast two-hybrid screen and identified the chromobarrel domain protein Mrg15 to interact with the Cap-H2 condensin subunit. Genetic interactions demonstrate that *Mrg15* function is required for Cap-H2-mediated unpairing of polytene chromosomes in ovarian nurse cells and salivary gland cells. In diploid tissues, transvection assays demonstrate that *Mrg15* inhibits transvection at *Ubx* and cooperates with Cap-H2 to antagonize transvection at *yellow*. In cultured cells, we show that levels of chromatin-bound Cap-H2 protein are partially dependent on Mrg15 and that Cap-H2-mediated homolog unpairing is suppressed by RNA interference depletion of Mrg15. Thus, maintenance of interphase chromosome compaction and homolog pairing status requires both Mrg15 and Cap-H2. We propose a model where the Mrg15 and Cap-H2 protein–protein interaction may serve to recruit Cap-H2 to chromatin and facilitates compaction of interphase chromatin.

CHROMOSOME structure is highly dynamic in proliferating cells as chromatin states must accommodate repeated rounds of replication, condensation, segregation, and decondensation. Although dramatic changes in chromosome morphology are usually associated with condensation of chromosomes in mitosis, dynamic three-dimensional (3D) spatial organization of interphase chromosomes is also thought to be important for gene regulation (Belmont 2006; Jackson 2010; Rajapakse and Groudine 2011). In some cell types, interphase chromosomes can maintain a Rabl conformation, while others arrange interphase chromosomes into discrete subnuclear compartments known as chromosome territories (Cremer and Cremer 2006; Lieberman-Aiden *et al.* 2009; Rajapakse *et al.* 2009). Recent evidence suggests that compaction of interphase chromosomes is sufficient to drive chromosome territories in *Drosophila* polyploid cells and that this is achieved through the activities of condensin II (Hartl *et al.* 2008b; Bauer *et al.* 2012). Condensin II activity is similarly required for axial compaction of mitotic chromosomes in a variety of systems (Shintomi and Hirano 2011; Green *et al.* 2012), and the regulation of mitotic condensin activity has been extensively studied (Bazile *et al.* 2010; Cuylen and Haering 2011). How condensin activity is regulated in interphase cells to modulate global chromosome organization remains unclear.

A characteristic of interphase chromosome organization is that there are extensive interactions between different chromosomes even though they are organized into globular territories (Sanyal *et al.* 2011). These *trans*-interactions can occur between homologous or nonhomologous sequences to

Copyright © 2013 by the Genetics Society of America
doi: 10.1534/genetics.113.153544
Manuscript received May 23, 2013; accepted for publication June 14, 2013
Supporting information is available online at http://www.genetics.org/lookup/suppl/doi:10.1534/genetics.113.153544/-/DC1.
Available freely online through the author-supported open access option.
[1]These authors contributed equally to this work.
[2]Corresponding author: Geisel School of Medicine at Dartmouth, Department of Genetics, 7400 Remsen, Hanover, NH 03755. E-mail: giovanni.bosco@dartmouth.edu

form local functional compartments or nuclear bodies (Sutherland and Bickmore 2009; Dundr 2012). In *Drosophila*, allelic interactions are favored due to extensive pairing of homologs in somatic cells, and the mechanisms through which this pairing is regulated have only recently been revealed (Bosco 2012). In addition to its chromosome compaction activity, condensin II also has been shown to be a potent antagonist of homologous chromosome pairing in somatic cells and in male meiosis (Hartl *et al.* 2008a,b; Bateman *et al.* 2012; Bauer *et al.* 2012; Joyce *et al.* 2012). That condensin II, and in particular the Cap-H2 condensin subunit, is important for functional *trans*-interactions is evidenced by *Drosophila* mutants that enhance transvection (Hartl *et al.* 2008a). Transvection is a specific type of pairing-sensitive process in interphase cells, which was first described by Ed Lewis in the 1950s (Lewis 1954). Transvection occurs when a regulatory site on one allele activates or represses the transcriptional state of its homologous allele (Kennison and Southworth 2002). This process is thought to be dependent on the proximity of the two homologous chromosomes in 3D space and therefore can be affected by chromosomal movements altering the homologs' proximity to each other. *Trans*-activation is presumed to occur by the productive interactions of enhancers and promoters on two different homologous chromosomes (Wu and Morris 1999; Kennison and Southworth 2002). *Trans*-repression has also been observed in *Drosophila*. In the case of the *Drosophila* bw^D mutation, a 2-Mb insertion of heterochromatic repeats functions to physically move the normally euchromatic bw^+ allele to a heterochromatic environment via *trans*-chromosomal interactions between the two *bw* allelic chromosomal regions (Henikoff and Dreesen 1989). Both *trans*-activation and *trans*-repression are similar in that both require homolog pairing to mediate regulation of gene expression of one allele by a second allele. Similarly, both *trans*-activation and *trans*-repression can also be hindered by chromosomal rearrangements that are thought to inhibit long/contiguous stretches of DNA homology along homologs. In mammalian systems, interchromosomal interactions are associated with gene regulation (Spilianakis *et al.* 2005; Lomvardas *et al.* 2006; Takizawa *et al.* 2008) and in some cases may explain sporadic reoccurring chromosomal translocations (Roix *et al.* 2003; Soutoglou *et al.* 2007). The underlying molecular mechanisms of these and other examples of chromosomal structural reorganization and movements in interphase cells are not well understood. In the *Drosophila* system, it has been proposed that the condensin II subunit, Cap-H2, provides a strong antipairing activity that normally antagonizes transvection (Hartl *et al.* 2008a). This condensin antipairing activity has also been shown in cultured *Drosophila* cells (Bateman *et al.* 2012; Joyce *et al.* 2012; Buster *et al.* 2013). A recent study showed that high levels of homolog pairing is maintained in interphase by active destruction of the Cap-H2 protein through the SCF^{Slimb} ubiquitin E3-ligase (Buster *et al.* 2013). Because RNA interference (RNAi) depletion or mutations of Cap-H2 lead to increased homolog pairing, it has been proposed that low levels of Cap-H2 protein in interphase nuclei must be important for modulating pairing status (Hartl *et al.* 2008a; Bateman *et al.* 2012; Bauer *et al.* 2012; Joyce *et al.* 2012; Buster *et al.* 2013). However, how Cap-H2 is activated in interphase cells to oppose homolog pairing has not been studied. Moreover, whether condensins play any antipairing function in systems other than *Drosophila* is not known. It has been proposed that the axial compaction activity provided by condensin II is sufficient for its antipairing activity by sequestering sequences into interchromosomal globules and thus indirectly antagonizing *trans*-interactions between homologs and heterologous chromosomes (Hartl *et al.* 2008a; Bauer *et al.* 2012).

Condensin protein complexes were originally identified as having mitotic chromosome condensation activity *in vitro* (Hirano *et al.* 1997). Subsequent work has shown that condensins also play diverse roles in interphase chromosomes (Wood *et al.* 2010; Zaidi *et al.* 2010). Both condensin I and II contain two **s**tructural **m**aintenance of **c**hromosomes subunits, SMC2 and SMC4, that are highly conserved and contain ATPase domains (Hirano and Hirano 2006; Hirano 2006). Mammalian condensin I contains Cap-H, Cap-D2, and Cap-G while condensin II contains Cap-H2, Cap-D3, and Cap-G2 (Ono *et al.* 2003; Yeong *et al.* 2003). Interestingly, a *Drosophila* Cap-G2-encoding gene has not been identified. Condensin I and II do not completely overlap in function as it has been shown that condensin II contributes to axial shortening of chromosomes whereas condensin I promotes lateral compaction (Shintomi and Hirano 2011; Green *et al.* 2012). Similarly, *Drosophila* condensin II has recently been shown to drive axial shortening and unpairing of interphase polyploid chromosomes (Bauer *et al.* 2012). In cultured *Drosophila* cells, this antipairing activity has been shown to be dependent on condensin II-specific subunits but not condensin I-specific subunits (Joyce *et al.* 2012; Buster *et al.* 2013).

To better understand how Cap-H2 may be targeted to chromatin and its activity regulated, we wanted to take a nongenetic approach to uncover as-yet-unidentified Cap-H2-interacting proteins. Such novel interacting proteins may serve to modulate *in vivo* condensin activities and/or recruit condensin activity to local regions of the genome. We first performed a yeast two-hybrid screen to identify candidates that physically interacted with the *Drosophila* Cap-H2 protein. We show that the *Drosophila* homolog of the human *Mortality Factor 4* (*Morf4*), Mrg15, was identified as physically and genetically interacting with Cap-H2.

Materials and Methods Yeast two-hybrid complementary DNA expression library screening

Total RNA was extracted from ovaries of the *Drosophila melanogaster* strain *cn bw sp* (Bloomington Stock Center #4455) using Trizol reagent (Invitrogen). Poly-A^+ RNA was enriched using the Poly-ATtract mRNA Isolation System (Promega). Subsequent complementary DNA (cDNA)

library construction and screening was performed using BD Matchmaker Library Construction and Screening Kits (BD Biosciences-Clontech). Briefly, poly(A) RNA was used to synthesize first-stranded cDNA with CDS III oligo(dT) primer and the BD SMART III primer, and the synthesized first-strand cDNA molecules were flanked at 5′ and 3′ ends by BD SMART III and CDS III anchors, respectively. The cDNA was amplified by PCR with primers of BD SMART III and CDS III anchors to generate a double-stranded cDNA library. The cDNA library was transformed into yeast strain AH109 together with linear vector pGADT7-Rec and Cap-H2 bait construct in vector pGBKT7 to screen the library according to the kit manual. The transformed yeast cells were selected on standard defined medium lacking adenine, histidine, leucine, and tryptophan. The number of total possible transformants was calculated by plating dilution aliquots of each transformation reaction on double-dropout plates lacking leucine and tryptophan, which merely selected for the presence of the bait (pGBKT7) and prey (pGADT7-Rec) plasmids; in this case, growth was not dependent on two-hybrid-interacting proteins. Individual colonies that supported growth on quadruple dropout plates were collected and restreaked on selective media, and putative cDNA inserts were PCR-amplified with primers of BD SMART III and CDS III anchors, as above. These PCR products were transformed back into AH109 together with linear vector pGADT7-Rec and Cap-H2 bait construct in vector pGBKT7, as above. PCR products that gave high levels of transformants on quadruple dropout media were analyzed further by PCR amplification of three different clones to confirm single insert size and by DNA sequencing. Clones with more than one insert were retransformed into yeast as above, and clones that could not be sequenced were discarded. Sequences mapping to *Drosophila* open reading frames were identified by BLAST searches.

S2 cell transfection, protein extraction, and immunoprecipitations

Mrg15 and Cap-H2 cDNAs were cloned in pMT/V5-His-TOPO (Invitrogen), which has metal-inducible *Drosophila* methallothionein (MT) promoter to drive gene expression. To make a C-terminal-tagged pMT > Cap-H2-EGFP, first EGFP was cloned into pMT using *Eco*RI to *Not*I restriction sites. Cap-H2 cDNA was PCR-amplified using primers CGGGGTACCatggagcgggttttgcc and CCGGAATTCcttcaggcgggctgtcg, where the lowercase nucleotides are *Cap-H2* sequences, digested with *Kpn*I and *Eco*RI and cloned in frame to EGFP. *Drosophila* S2 cells were transfected using an Amaxa Nucleofector 2b (Lonza) with 2 μg total plasmid DNA. For immunoprecipitations, 0.25 mg of mouse monoclonal anti-V5 antibody (Invitrogen) was bound to equilibrated ProteinG-coupled Sepharose (Sigma-Aldrich) by gently rocking overnight at 4° in 0.2 M sodium borate. For GFP immunoprecipitations, GFP-binding protein (GFPBP) (Rothbauer *et al.* 2008) was fused to the Fc domain of human IgG (pIg-Tail) (R&D Systems), tagged with His6 in pET28a (EMD Biosciences), expressed in *Escherichia coli*, and purified on Talon resin (Clontech) according to the manufacturer's instructions. GFPBP was bound to ProteinA-coupled Sepharose, cross-linked to the resin using dimethylpimelimidate, and rocked for 1 h at 22°, and the coupling reaction was quenched in 0.2 M ethanolamine (pH 8.0) and rocked for 2 h at 22°. Antibody or GFPBP-coated beads were washed 3× with 1.5 ml of cell lysis buffer (CLB; 100 mM Tris, pH 7.2, 125 mM NaCl, 1 mM DTT, 0.1% Triton X-100, 0.1 mM PMSF). Transfected S2 cells were induced to express EGFP, V5, Mrg15-V5, or Cap-H2-EGFP with 0.35 mM CuSO4. After 24 h, cells were lysed in 0.5 ml of CLB, clarified by centrifugation, and then diluted to 2–5 mg/ml in CLB. Antibody-coated beads or GFPBP crosslinked beads were mixed with lysate for 40 min at 4°, washed 3× with CLB, and then boiled in Laemmli sample buffer. Cap-H2-EGFP was detected on immunoblots with mouse monoclonal anti-GFP (JL-8 Clontech). In all cases, 25 μl of ProteinG beads with either a saturating amount of cross-linked GFPBP or preconjugated with 0.25 mg of anti-V5 was used. For immunoblots, anti-V5 was used at 1:500 dilution.

S2 cell RNAi and chromatin fractionation

Double-stranded RNA (dsRNA) was made to a noncoding region of the pBlueScript SK plasmid (control) and to *Mrg15* sequences as follows: control pBlueScript SK DNA was PCR-amplified using primers 5′-TAATACGACTCACTATAGGG ATGGATAAGTTGTCGATCG-3′ and 5′-TAATACGACTCACTATAGGG ACCAGGTTCACATGCTTGCG-3′. Mrg15 DNA was amplified from Oregon R genomic DNA using primers 5′-TAATACGACTCACTATAGGG ATCTCGTGCCTCGACGC-3′ and 5-TAATACGACTCACTATAGGG CACTGGTCGATTTCACGG-3′. The underlined nucleotides denote the T7 RNA polymerase promoter sequence, and dsRNA was made using the Ribomax Large Scale RNA Production System (Promega) according to manufacturer instructions. S2 cells were transfected by Amaxa nucleofection (Lonza) according to manufacturer instructions with 2 μg pMT-Cap-H2-V5 and treated every other day for a total of 6 days with 10 μg of dsRNA directed against pBlueScript SK as a control or against Mrg15 messenger RNA (mRNA) sequence. Induction of Cap-H2-V5 was done on day 5 using 1 mM final concentration of $CuSO_4$. Cells were harvested and 20 μg of total cell lysate protein was analyzed by Western blot using mouse anti-V5 (Invitrogen) at 1:500, rabbit anti-Mrg15 at 1:500 (Kusch *et al.* 2004), and mouse anti-Lamin Dm0 at 1:1000 (ADL84.12-c, Developmental Studies Hybridoma Bank); each antibody detects only one major band (Supporting Information, Figure S5). Cells treated with dsRNA targeting Mrg15 exhibit >75% depletion of endogenous Mrg15 protein, relative to nuclear Lamin (Figure S5). This was consistent through four biological replicates. Cells were prepared into cytoplasmic, nuclear, and chromatin fractions as previously described (Wysocka *et al.* 2001). Total protein recovered from each fraction was quantified by Bradford's assay, 20 μg of protein from each fraction was immunoblotted for Cap-H2-V5 or Cap-H2-EGFP and Lamin, and

specific bands were quantitated by densitometry after background subtraction using ImageJ. The levels of chromatin-bound epitope-tagged Cap-H2-V5 or Cap-H2-EGFP for control RNAi and Mrg15 RNAi were calculated with the following formula: [(chromatin fraction Cap-H2/chromatin fraction Lamin)/whole-cell lysate Cap-H2/whole-cell lysate Lamin) for Mrg15 dsRNA-treated cells]/[(chromatin fraction Cap-H2/chromatin fraction Lamin)/whole-cell lysate Cap-H2/whole-cell lysate Lamin) for control dsRNA-treated cells]. Four biological replicates were done, and an average fold enrichment was calculated. *P*-value was calculated by two-tailed *t*-test assuming unequal variance in Microsoft Excel.

Chromosome length measurements in Kc_{167} cells

dsRNA depletion of Mrg15 and Cap-H2 was done as described above for S2 cells. Primers for Cap-H2 RNAi were as follows (underlined DNA are T7 RNA polymerase sequences): 5′-TAATACGACTCACTATAGGG ACCGGAGAAAAACGAGCGCAGGCC and 5′-TAATACGACTCACTATAGGG GGGATCCACTCTCGTGC. Image *z*-stacks were acquired with a Nikon A1RSi confocal microscope with Plan Apo 100× oil immersion objective lens. Three-dimensional distances between pairwise probe sets were made using the 3D distance measurement tool in Nikon elements 4.0 software package. Pairwise distance measurements were made by marking the centroid of each respective FISH focus. Statistical analyses were performed using a Student's *t*-test in Microsoft Excel. BAC clones (CHORI BACPAC Resources) for FISH were as follows: X1, BACR30C13 and BACR18F10; X2, BACR20K01 and BACR35A18; X3, BACR11C13 and BACR07F15; 2L(1) BACR30M19 and BACR29P12; 2L(2), BACR15P08 and BACR14I17. Table S4 reports the number of nuclei sampled and other details for each experimental treatment.

Salivary gland suppression

We used two *Drosophila* stocks in which we could observe LacI-GFP spot localization: one line, we refer to as the "spots" line, is homozygous for 256× LacO arrays at cytological location 60F, *hs83 > LacI-GFP* on the second chromosome and *Cap-H2^{EY09979}* (Bloomington Stock Center #17627), *Hsp70 > Gal4* in which both the LacI-GFP and Gal4 are under heat-shock control. The second line, which we refer to as "donut," is identical to the "spots" line except it does not contain *Cap-H2^{EY09979}* and thus Cap-H2 cannot be overexpressed. The *UAS > Mrg15*-RNAi line is Vienna Drosophila RNAi Center (VDRC) #v43802. The *Mrg15^{j6A3}* (Bloomington Stock Center #10290) is a *P*-element insertion. Crosses were done on yeast/molasses/cornmeal media and kept at 25°. After 5–6 days, the cross larvae were heat-shocked at 32° overnight. Third instar larvae were dissected in PBS with 0.1% Triton-X (PBT), and glands were fixed for 10 min in PBS, 4% formaldehyde. Glands were rinsed three times with PBT and stained 10 min with DAPI (0.1 μg/μl final) in 1 ml of PBS with 0.005% Triton-X followed by two 10-min washes in PBT. Initial quantification of the percentage of polytene was done visually by DAPI staining using a Nikon Eclipse E800 40× objective (Figure S1, Table S2). Further imaging was done using a Zeiss LSM 510 Meta Confocal at 63× with 1-μm slices, and measurements of the number of GFP spots and distance were done using the LSM image browser software (release 4.0). At least three different glands (biological replicates) were imaged for the GFP spot counting. In cases where the number of GFP spots and distance between spots was measured, the same nuclei were used for both calculations. All Student *t*-tests were done using two-tailed and two samples with equal variance as the parameters in Microsoft Excel.

Quantitative PCR for *Mrg15* mRNA levels was done by extracting RNA with Qiagen RNeasy Mini Kit from heat-shocked larvae resulting from "spots" crossed to *UAS > Mrg15*-RNAi line (VDRC #43802) or "spots" crossed to *Oregon-R* (control). Primers for *Mrg15* were 5′-GAAAA TAAAATGGGAGAAGTAAAACC-3′ and 5′-GGTTTTGTTTT CAGAACCTTGG-3′. First-strand cDNA was made with Verso cDNA synthesis kit (Thermo Scientific #AB-1453/B). mRNA levels were amplified using iQ SYBR Green Supermix (Bio-Rad) and Stratagene Mx3005P (Agilent Technologies) along with MxPro qPCR software. Primers for *RpL32* were 5′-CCTTCCAGCTTCAAGATGACC-3′and 5′-ACTCTGTTGTC GATACCCTTGG-3.′ Levels of *Mrg15* mRNA for each sample were calculated relative to RpL32 as follows: (1 + *Mrg15* efficiency)$^{(\Delta CT\ Mrg15\ (control - treated))}$/(1 + *RpL32* efficiency)$^{(\Delta Ct\ Rpl32\ (control - treated))}$, as recommended by the manufacturer (Bio-Rad).

Nurse-cell FISH and spot quantitation

Strains used: *P*-element hypomorph for *Smc4* (*gluon*) *Smc4^{k08819}/CyO* (Bloomington Stock Center #10831; in the text we refer to this allele as *Smc4^{k08819}*) and the *Smc4$^{88-82}$/CyO* have been described (Cobbe *et al.* 2006); the *Cap-H2* mutation *Cap-H2$^{Z3-0019}$* and *Df(3R)Exel6195/TM6 B* deficiency deleting the Cap-H2 locus was described (Hartl *et al.* 2008a); the deficiency deleting *Mrg15* was *Df(3R)BSC741* (Bloomington Stock Center #26839), which has breakpoints at 88E8 and 88F1.

FISH probe preparation: BAC clones (CHORI BACPAC Resources) were used for the detection of the 34D region (RP98-16P12, RP98-48E2, and RP98-30I21), the *Ubx* region (RP98-24L18 and RP98-28H1), and the CapH 2 region (RP98-29B06). DNA was labeled and tissues were prepared for hybridizations as previously described (Hartl *et al.* 2008a; Bauer *et al.* 2012).

Microscopy and spot analysis: Stage 6/7 egg chambers were imaged on a Zeiss LSM 510 Meta Confocal with an objective of 40× with *z*-slices of 1 μm. Spots were manually counted for each probe.

Nurse-cell RNAi depletion of Mrg15 and polytene unpairing

The maternal α-tubulin67C driver was used to express female germline-specific Gal4VP16 (*Matα4-GAL-VP16*; Bloomington

Stock Center 7062 and 7063) (Hacker and Perrimon 1998). Virgin *Matα4-GAL-VP16* females were crossed to males from a TRiP line capable of expressing an RNA-hairpin targeting the Mrg15 transcript in the germline (Bloomington Stock Center 35241: *y[1] sc[*] v[1]*; *P[y[+t7.7]v[+t1.8]=TRiP.GL00128] attP2/TM3*, *Sb[1]*). One- to 3-day-old Sb^+ F_1 females were collected and fattened on yeast paste for 2 days at 25°. Ovaries were dissected as described above for FISH and processed for DNA FISH and anti-Mrg15 immunofluorescence. As controls, F_1 progeny from *Matα4-GAL-VP16* females crossed to *Oregon-R* or a different TRiP line targeting the *Set2* gene (Bloomington Stock Center 33076): *y[1] sc[*] v[1]*; *P[y[+t7.7] v[+t1.8]=TRiP.HMS00583]attP2*). Endogenous Mrg15 protein germline-specific depletion was confirmed by whole-mount immunofluorescence of egg chambers as follows: Mrg15-TRiP and control ovaries were incubated with rabbit polyclonal anti-Mrg15 serum at 1:100 and goat anti-rabbit Alexa Fluor 488 (Invitrogen) at 1:200. Image *z*-stacks (0.5 μm *z*-step size) were acquired with a Nikon A1RSi confocal microscope with Plan Apo 60× oil immersion objective lens, and relative amounts of protein were measured by drawing a line across a two-dimensional confocal *z*-slice of an entire stage 5/6 egg chamber. Gray-scale pixel intensity values across two follicle cells and two nurse cells (~50–60 μm total distance) for DAPI and anti-Mrg15 were acquired with the National Institutes of Health ImageJ analysis tool "Plot Profile." Relative protein levels in RNA-hairpin-expressing and control egg chambers were normalized to the somatic follicle cell Mrg15 immunofluorescence signal (the *Matα4-GAL-VP16* driver is germline specific, and therefore protein levels in somatic follicle cells are unaffected in both control and TRiP lines).

Transvection assays

These assays were done as previously described (Hartl *et al.* 2008a), and stocks were a gift from Chao-Ting Wu. Scoring of *Ubx* phenotypes and *yellow* pigmentation transvection phenotypes was done blind where multiple individuals were not aware of the genotypes. Briefly, *Ubx* crosses were done at 25° and brooded twice. The $Ubx^{Cbx\text{-}1}$ Ubx^{1}/TM6B *Tu*, *Hu*, *e* was crossed to Oregon-R or $Mrg15^{j6A3}$/TM6B *Tu*, *Hu*, *e*. The rearrangement of $Ubx^{Cbx\text{-}1}$ Ubx^{1} (BTD in Figure S3) was #800.7 BTD24/MRS, *Sb* T(2;3) 50C1/C4; 81F. Wings were chosen from females with no balancers with genotypes: $Ubx^{Cbx\text{-}1}$ Ubx^{1}/+ and $Ubx^{Cbx\text{-}1}$ $Ubx^{1}/Mrg15^{j6A3}$. Class A wings had loss of posterior tissue, typical of the $Ubx^{Cbx\text{-}1}$ Ubx^{1}/+ background but clearly not wild type; class B had a large loss of posterior tissue and blistering of the wing. See Figure 7, B and C, for representative class A and B wing images. For transvection at the *yellow* gene, methods and alleles were as previously described (Geyer *et al.* 1990; Morris *et al.* 1999; Hartl *et al.* 2008a). The following crosses were done: First, y^{82f29}/y^{82f29}; $Cap\text{-}H2^{Z3\text{-}0019}/TM6B$, *Hu* females were crossed to w^{1118}/Y; $Mrg15^{j6A3}/TM3$ *Sb* males and F_1 y^{82f29}/Y; $Mrg15^{j6A3}/TM6B$, *Hu* males were collected. These y^{82f29}/Y; $Mrg15^{j6A3}/TM6B$, *Hu* males were crossed to females from three different lines: (1) $y^{1\#8}/y^{1\#8}$; $Cap\text{-}H2^{Z3\text{-}0019}/TM6B$, (2) $y^{1\#8}/y^{1\#8}$; $Df(3R)Exel6159/TM6B$, and (3) $y^{1\#8}/y^{1\#8}$. For additional controls, $y^{1\#8}/y^{1\#8}$; $Cap\text{-}H2^{Z3\text{-}0019}/TM6B$ and $y^{1\#8}/y^{1\#8}$; $Df(3R)Exel6159/TM6B$ were crossed to y^{82f29}/Y males. For each genotype, between 10 and 15 independent crosses were established, each with two females and two males. Each cross was brooded three times for 3 days, after which parental flies were then discarded. Adult F_1 female progeny were collected daily (over a period of 15 days) and held in another vial for 3 days at 25°; then the abdominal stripe pigmentation of flies from each genotype that eclosed on the same day and arose from the same brood was scored relative to each fly. To prevent biasing the scorer, genotypes were concealed until after scoring completion, and females were scored blind by two individuals, as previously described (Hartl *et al.* 2008a). All female progeny with relevant genotypes were scored and placed into four body-pigmentation classes. Note that only abdominal stripes were considered in pigmentation scoring and not interstripe abdominal cuticle or thoracic cuticle. This pigmentation scale was developed independently of others and should not be compared to those previously described. Class 1 had no/little detectable pigmentation equal to $y^{1\#8}/y^{1\#8}$ and y^{82f29}/y^{82f29} homozygotes (Morris *et al.* 1999). Class 2 had moderate pigmentation; class 3 had moderate-to-darkly pigmented posterior-most stripes only; class 4 had darkly pigmented posterior stripes and some dark pigmentation of more anterior stripes (for examples, see Figure 8 and details in its legend). Subtle variation within each class was noted. Transvection experiments at the *yellow* locus were done with an $Mrg15^{j6A3}$ line (a *P*-w^+ insertion) that was crossed to a w^{1118} female, and w^+ females were backcrossed to w^{1118} males for seven generations, selecting for w^+ female progeny, and thus allowing female meiotic recombination to occur on all chromosomes.

Results

Cap-H2 and Mrg15 proteins interact

Cap-H2 is required for polytene chromosome unpairing as well as unpairing of homologous sequences in cultured *Drosophila* cells (Hartl *et al.* 2008a; Bauer *et al.* 2012; Joyce *et al.* 2012; Buster *et al.* 2013). Although this activity is dependent on other condensin genes, such as *SMC4* and *Cap-D3*, it is not known what other factors may function to recruit and/or activate this condensin activity on chromatin. To identify proteins that interact with Cap-H2 protein, a yeast two-hybrid screen was done using *Cap-H2* cDNA fused to the GAL4 DNA-binding domain (GAL4BD) as bait protein. Because the primary phenotypes observed in *Cap-H2* mutants are in the ovary, we reasoned that potential regulators of *Cap-H2* would be most abundant in the ovarian transcriptome. Therefore, a cDNA library from *Drosophila* ovarian mRNA was constructed as GAL4-activation domain fusions and was used as prey protein. Of ~10^5 total putative cDNA clones that were plated, 124 were able to grow under selection that required a bait–prey interaction. Clone inserts were PCR-amplified using universal vector primers and recloned

into the prey vector by homologous recombination in yeast. Of these, 84 clones retested as positive and inserts were sequenced (Table S1). We found that a disproportionate number of clones encoded known or predicted ribosomal proteins (21 clones) and translation regulatory factors (7 clones). In addition, *yolk protein 1* (CG2985) was represented by 7 independent clones. We speculate that these interactions may be nonspecific, and they are overrepresented because of the vast abundance of ovarian transcripts encoding protein synthesis, chorion, and yolk proteins.

Two additional genes were represented by three or more Cap-H2-interacting clones: *Rack1* (CG7111) was recovered in seven clones while *Mrg15* (CG6363) was recovered in three clones (Table S1). In an *in vitro* protein translation system, Rack1 protein exhibited only weak protein–protein interactions with Cap-H2, and three different *Rack1* mutants ($Rack1^{1.8}$, $Rack1^{EY00128}$, $Rack1^{EE}$) failed to modify nurse cell polytene phenotypes caused by *Cap-H2* and *Smc4* mutations (data not shown). Therefore, we did not pursue *Rack1* as an interactor of condensin function. An interaction between Cap-H2 and Mrg15 proteins previously was identified by a large-scale protein interaction screen (Giot *et al.* 2003). Here, we report further analysis of the Cap–H2 interaction with Mrg15.

The *Mrg15* gene is found in all metazoans. The Mrg15 homolog in the budding yeast is *Eaf3*, and the human homolog is *Morf4* (Bertram *et al.* 1999; Bertram and Pereira-Smith 2001; Chen *et al.* 2010). The yeast Eaf3 protein can bind histone H3 monomethyl, dimethyl and trimethyl lysine-36 as well as H3 trimethyl lysine-4 (Joshi and Struhl 2005). The human Morf4 chromodomain binds to H3 dimethyl and trimethyl lysine-36 (Zhang *et al.* 2006). The *Drosophila* Mrg15 protein is enriched at sites of active gene expression (Filion *et al.* 2010), and it has been reported to bind H3 trimethyl lysine-36 and monomethyl and dimethyl lysine-20 on histone H4 (Moore *et al.* 2010). The MRG domain is less well characterized, but it has been reported to contain HLH and leucine-zipper motifs, suggesting that the MRG domain may mediate interactions with other proteins (Bertram and Pereira-Smith 2001; Chen *et al.* 2010). A previously described Mrg15 protein-binding consensus sequence (FxLP) has been determined through MRG domain structure–function studies (Xie *et al.* 2012). Interestingly, a FKLP sequence exists within all four reported *Drosophila* Cap-H2 protein isoforms.

The protein domain illustration in Figure 1A shows the full-length 424-amino-acid protein and portions of Mrg15 that were recovered in three independent clones from the yeast two-hybrid screen. All three of the interacting Mrg15 cDNA inserts contain the C-terminal MRG domain while one clone is lacking the entire N-terminal chromodomain, suggesting that the MRG domain is sufficient for the interaction with Cap-H2. C-terminal deletions were constructed and tested, and these did not exhibit any interaction with the GAL4BD-Cap-H2 bait (Figure 1B and data not shown), further demonstrating that the MRG domain is necessary for a two-hybrid interaction with Cap-H2. These data suggest that amino acids 256–424 are necessary for the Mrg15 protein interaction with Cap-H2.

The interaction between Mrg15 and Cap-H2 was tested in cell culture using S2 cells. Both *Mrg15* and *Cap-H2* cDNA clones were inserted into pMT expression vectors under the control of the metallothionein promoter. pMT-Mrg15-V5 contains a V5-epitope C-terminal tag while the pMT-Cap-H2-EGFP contains a C-terminal EGFP or GFP. Cotransfection of pMT-Cap-H2-EGFP and an empty vector control (pMT with no insert) resulted in a Cap-H2-EGFP band to immunoprecipitate (IP) with recombinant GFPBP (Rothbauer *et al.* 2008) while EGFP was detected on an immunoblot (IB) with anti-GFP antibody (Figure 1C). The same IP reactions were immunoblotted with anti-V5 antibodies and did not yield detectable Cap-H2-EGFP bands (Figure 1C, bottom). When pMT-EGFP was cotransfected with pMT-Mrg15-V5, GFPBP was able to IP EGFP but not Mrg15-V5 (Figure 1D). In these same extracts, anti-V5 antibodies were able to IP Mrg15-V5 but not EGFP alone (Figure 1D, right). These data show that in S2 cell extracts anti-V5 antibodies cannot IP EGFP and GFPBP cannot IP overexpressed Mrg15-V5 protein. Next we co-transfected pMT-Cap-H2-EGFP with pMT-Mrg15-V5. In these extracts expressing Cap-H2-EGFP and Mrg15-V5, GFPBP was able to IP both Cap-H2-EGFP and Mrg15-V5 (Figure 1E, top). In the reciprocal experiment, anti-V5 antibodies were able to IP both Mrg15-V5 and Cap-H2-EGFP (Figure 1E, bottom).

Because proteins are likely overexpressed from the pMT-plasmid, we tested whether endogenous Mrg15 protein could IP with overexpressed Cap-H2-EGFP. First, we transfected S2 cells with either pMT-EGFP alone or pMT-Cap-H2-EGFP alone. GFPBP immunoprecipitations did not detect any protein bands at ~175 kDa in the pMT-EGFP only cells (Figure 1F, top left), whereas GFPBP could IP an ~175-kDa protein band from cells transfected with pMT-Cap-H2-EGFP (Figure 1F, top right). In cells expressing pMT-EGFP alone, anti-GFP immunoblots (IB:GFP) specifically recognize EGFP at ~27 kDa from a GFPBP IP and do not detect a polypeptide at the predicted ~175-kDa size for Cap-H2-EGFP (Figure 1F, left). This again demonstrates that anti-GFP immunoblots specifically recognize GFP-tagged proteins only. In cells transfected with pMT-EGFP alone, GFPBP was not able to IP endogenous Mrg15 detected at ~50 kDa, even though 10% of total input extract used has abundant levels of Mrg15 protein (Figure 1F, bottom left). In cells transfected with pMT-Cap-H2-EGFP, GFPBP was able to IP both Cap-H2-EGFP and endogenous Mrg15 (Figure 1F, bottom right).

Taken together with the yeast two-hybrid interaction these co-immunoprecipitation experiments suggest that Cap-H2 and Mrg15 proteins interact. This observation is consistent with a previously reported large-scale *Drosophila* yeast two-hybrid screen demonstrating a Cap–H2–Mrg15 protein interaction (Giot *et al.* 2003).

Mrg15 is required for Cap-H2-mediated salivary gland polytene dispersal

To ask if *Mrg15* and *Cap-H2* interact *in vivo*, a functional genetic test was done using salivary gland cells. Wild-type larval salivary gland nuclei are polyploid and contain

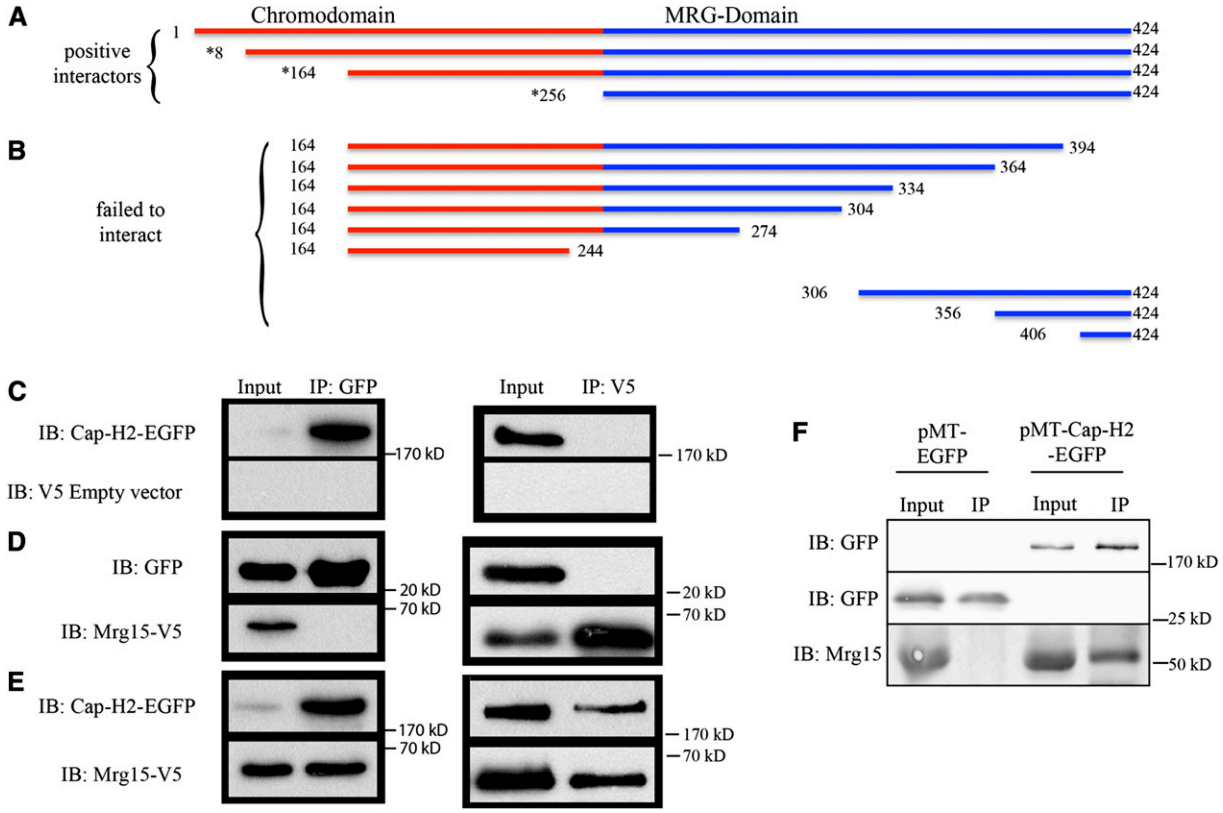

Figure 1 Mrg15 protein interacts with Cap-H2. (A) Linear protein map showing Mrg15 (not to scale). The red line shows the chromo-barrel domain and the blue line shows the MRG domain. Numbers represent amino acid positions relative to the full-length 424-amino-acid predicted protein (GenBank accession AAF55161). Three Mrg15 clones were recovered from a yeast two-hybrid screen (asterisk) and the full-length proteins were found to interact. (B) Linear depictions of the constructs that failed to interact with Cap-H2 in the yeast two-hybrid assay. (C–E) Immunoprecipitations (IP) were done with GFP-binding protein (IP:GFP) or anti-V5 (IP:V5), and 10% of IP supernatant from S2 cell extracts were immunoblotted (IB) with anti-GFP (IB:GFP) or anti-V5 (IB:V5). (C) S2 cells cotransfected with pMT-Cap-H2-EGFP and pMT(empty vector). (D) Cells cotransfected with pMT-EGFP and pMT-Mrg15-V5. (E) Cells cotransfected with pMT-Cap-H2-EGFP and pMT-Mrg15-V5. (F, top) Cells transfected with pMT-Cap-H2-EGFP (right) produce a protein band at ~175 kDa that is immunoprecipitated by GFP-binding protein and detected by anti-GFP (IB:GFP). Cells transfected with pMT-EGFP (left) do not produce a protein band at ~175 kDa on immunoblots probed with anti-GFP. Middle panel: Cells transfected with pMT-EGFP (left) produce a GFP band at ~27 kDa, while cells transfected with pMT-Cap-H2-EGFP (right) do not produce an ~27-kDa protein band. (Bottom) Cells transfected with pMT-EGFP (left) have endogenous Mrg15 protein that does not IP with GFP-binding protein. GFP-binding protein can IP endogenous Mrg15 from cells transfected with pMT-Cap-H2-EGFP (right).

1000–2000 copies of each chromosome arranged in register to form a structure called polytene chromosomes where chromatids and homologs are paired in a homology-dependent manner. We previously have shown that *Cap-H2* overexpression in the larval salivary gland was sufficient to drive unpairing of polytene chromosomes, and this unpairing activity was completely suppressed by *Cap-D3* loss-of-function mutations (Hartl *et al.* 2008a). We tested whether *Mrg15* function was also necessary for this Cap-H2-mediated disassembly of salivary gland chromosomes. The LacO/LacI-GFP system (Vazquez *et al.* 2002) allows visualization of the pairing status of a single locus (the exogenous LacO array) in the genome. In salivary gland cells expressing wild-type levels of *Cap-H2*, there is one GFP spot or band because polytene chromosomes have all homologous sequences paired (Hartl *et al.* 2008a), and transgenic lines carrying *UAS > Mrg15-RNAi* similarly exhibit one large LacI-GFP spot or polytene band (Figure 2, A–C). In larvae containing *Hs > Gal4, UAS > Cap-H2* chromosomes become nonpolytene, and homologs and sister chromatids unpair and result in multiple GFP spots after heat-shock induction (Figure 2, D–F). We previously demonstrated that this *Cap-H2* overexpression phenotype could be suppressed by mutations in *Cap-D3*, suggesting that this polytene unpairing phenotype could be modulated by altering genetic factors (Hartl *et al.* 2008a). Here, we extend this observation by demonstrating that *in vivo* RNAi to *Cap-D3*, *Cap-H2*, or *Smc4* also suppresses the salivary gland *Cap-H2* overexpression phenotype (Figure S1, Table S2). To test whether suppression could also be achieved by RNAi, we used UAS > RNAi to other condensins and condensin-interacting genes: RNAi targeting of *Cap-G*, *Cap-H* (*barren*), *Smc3*, *Smc5*, and *Polo kinase*. These transgenic lines gave minimal to partial rescue of the polytene dispersal phenotype (Figure S1), although at present it is unclear how RNAi depletion of Smc3 or Smc5 results in rescue. UAS > RNAi transgenes targeting *Cap-D2*,

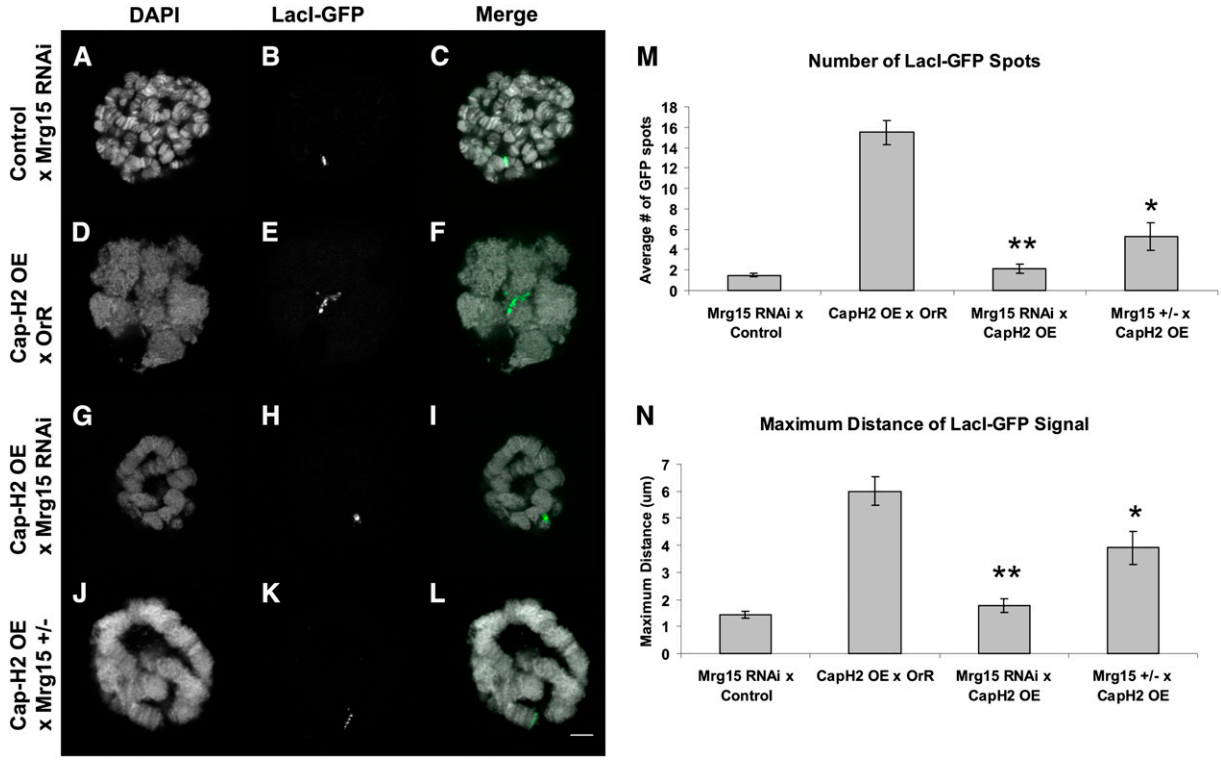

Figure 2 *Mrg15*-RNAi suppresses *Cap-H2* overexpression phenotypes in salivary glands. (A–C) Single salivary gland nucleus of a control *UAS > Mrg15-RNAi/+*, *Hs > LacI-GFP/+*, *LacO (60F)/+*; *Hs > Gal4/+*. (D–F) Cap-H2 overexpression (OE) line crossed to Oregon-R resulting in larvae as follows: *Hs > LacI-GFP/+*, *LacO (60F)/+*; *Hs > Gal4/+*, and *UAS > Cap-H2^{EY09979}/+*. (G–I) Cap-H2 overexpression line crossed to a Mrg15-RNAi line resulting in larvae as follows: *UAS > Mrg15-RNAi/+*, *Hs > LacI-GFP/+*, *LacO (60F)/+*; *Hs > Gal4/+*, and *UAS > Cap-H2^{EY09979}/+*. (J–L) Cap-H2 overexpression in an *Mrg15^{j6A3}* heterozygous background resulted in larvae as follows: *Hs > LacI-GFP/+*, *LacO (60F)/+*; *Hs > Gal4/+*, *UAS > Cap-H2^{EY09979}/+*, and *Mrg15^{j6A3}/+*. The left column (A, D, G, and J) is the DAPI channel. The middle column (B, E, H, and K) is the GFP channel. The right column (C, F, I, and L) is a merge of the two channels with DAPI in white and GFP in green. The white scale bar in L indicates 5 μm. (M) The average number of GFP spots per nucleus and standard error are plotted. One asterisk indicates a *P*-value of 1.9×10^{-4}, and two asterisks indicate a *P*-value of 3.9×10^{-9} using a two-tailed, equal variance Student *t*-test. (N) The maximum distance between two GFP signals was calculated, and the average distance with standard error was plotted. Using the Student *t*-test, one asterisk indicates $P = 0.02$ and two asterisks indicate $P = 1.1 \times 10^{-6}$. For each genotype, $n = 10$ nuclei.

Smc1, *trithorax* (*trx*), *enhancer of zest* [*E(z)*], and *Tip60* had little or no significant suppression of the polytene dispersal phenotype (Figure S1). Together, these data support a model where Cap-H2 most likely functions in the context of the condensin complex to disperse polytene chromosomes since knockdown of other condensin subunits produces partial or complete suppression, consistent with previous observations suggesting that this is a condensin complex function (Hartl *et al.* 2008a; Bauer *et al.* 2012; Joyce *et al.* 2012; Buster *et al.* 2013). More importantly, this demonstrates that ds RNA expression in the salivary gland cells can be an effective assay for *Cap-H2*-interacting genes. We note that not all UAS-driven hairpin transgenes target efficient depletion of mRNA, and therefore for those genes where little or no effects were observed, we cannot exclude the possibility that these genes were not sufficiently depleted.

We used this *Hs > Gal4/UAS*>RNAi system to test whether *Mrg15* interacts with *Cap-H2*. When *UAS > Mrg15* RNAi alone is crossed to the heat-shock-driven Gal4, the polytene structure is maintained after heat shock, demonstrating that Mrg15 depletion alone does not impact polytene structure (Figure 2, A–C). This was apparent by qualitative DAPI polytene visualization as well as by LacI-GFP tethering to LacO arrays (Figure 2, A–C). By contrast, *Cap-H2* overexpression produced a nonpolytene phenotype as indicated by an average of 15 GFP spots (Figure 2, D–E and M). The introduction of *UAS > Mrg15* RNAi into the *Cap-H2* overexpression line suppressed the nonpolytene phenotype as indicated by one GFP signal (Figure 2, G–I). Using this LacI-GFP system, the number of distinct spots and the maximum distance between the two farthest spots was calculated (Figure 2, M and N). In larvae with *Mrg15* RNAi *Cap-H2* overexpression, both the number of GFP spots and the maximum distance between spots were reduced significantly compared to *Cap-H2* overexpression alone ($P < 10^{-8}$ and $<10^{-5}$, respectively). To confirm that this *Mrg15* RNAi line effectively depleted Mrg15, we measured *Mrg15* mRNA levels by quantitative RT-PCR. We found that the *Mrg15* RNAi larvae had Mrg15 mRNA levels that were 50 ± 6% ($P = 0.032$) that of control larvae not containing the *Mrg15* RNAi transgene (relative to *RpL32* mRNA levels; see *Materials and Methods*). This is consistent with a previous report

showing that this very same RNAi line can deplete Mrg15 mRNA by 10–36% in whole larvae (Zhang *et al.* 2010). It is also noteworthy that an *Mrg15* overlapping gene, *l(3)neo43* (CG14865), shares no sequence homology to the 332-bp predicted RNA hairpin produced by the *Mrg15*-RNAi line.

Given that a 50% RNAi depletion of *Mrg15* mRNA was sufficient to suppress the *Cap-H2* overexpression phenotype (Figure 2, G–I), this predicted that reducing the *Mrg15* gene dosage to half could also suppress the salivary polytene phenotype. An *Mrg15* mutant, $Mrg15^{j6A3}$, was also crossed into the LacO/LacI-GFP *Hs > Gal4*, *UAS > Cap-H2* overexpression line. Using qualitative polytene DAPI staining, we observed an intermediate degree of suppression (Figure 2, J–L); however, the number of spots was significantly reduced ($P < 10^{-4}$) as was the maximum distance between GFP foci ($P = 0.02$). This suggests that the *Cap-H2* overexpression phenotype is very sensitive to *Mrg15* dosage, and 50% reduction by RNAi or by a mutation in one allele can lead to suppression. Additionally, because both the RNAi transgene and the loss-of-function mutant independently produce similar suppression of the Cap-H2 gain-of-function phenotype, it is unlikely that this suppression is caused by genetic background effects. Therefore, this suggests that *Mrg15* function is required *in vivo* for *Cap-H2*-mediated salivary gland polytene unpairing.

Mrg15 mutants enhance condensin II partial loss of function in ovarian nurse cells

In wild-type egg chambers, polyploid nurse cells undergo a transition from the polytene structure to nonpolytene during stage 5 (Dej 1999; Dej and Spradling 1999). This developmentally regulated chromosome reorganization is dependent on *Cap-H2*, *Smc4*, and *Cap-D3*, and thus we used this polytene-to-nonpolytene transition to test whether Mrg15 was also required. We used FISH with probes spanning ~350 kb to each of three different genomic locations at the *Ubx*, *Cap-H2*, and 34D loci. Confocal 3D images of stage 6/7 egg chamber nurse cells were acquired, and the number of discrete FISH signals in each nurse cell nucleus for each probe is a direct measure of chromatid and homolog pairing within the polytene structure (Dej 1999; Hartl *et al.* 2008a; Bauer *et al.* 2012). In Oregon-R stage 6/7 egg chambers, we detected 15–17 spots per wild-type nurse cell, depending on the probe used (Figure S2). Homozygous mutant *Cap-H2* nurse cells show complete polytene structure, have only one large detectable FISH spot, and therefore were not useful for testing enhancers of nurse cell polytene structure (Hartl *et al.* 2008a). To assay for a genetic interaction, we desired a sensitized background that is not completely polytene. Double-heterozygous mutations in the condensin II complex ($SMC4^{k08819}$/+; $Cap\text{-}H2^{Z3\text{-}0019}$/+) give an intermediate phenotype in nurse cells (Hartl *et al.* 2008a) and therefore were ideal for use in our assay. Furthermore, this double-heterozygous phenotype can be enhanced by an additional heterozygous mutation in the *Cap-D3* gene and suppressed by a heterozygous mutation in the *Slimb* E3-ubiquitin ligase (Hartl *et al.* 2008a; Buster *et al.* 2013). Therefore, the $SMC4^{k08819}$/+; $Cap\text{-}H2^{Z3\text{-}0019}$/+double-heterozygous line is ideal for testing genetic interactors. We used this sensitized genetic background to test for interactions between Cap-H2 and Mrg15 in ovarian nurse cells.

If Mrg15 is working with Cap-H2 to unpair polytenes, then a mutation in Mrg15 should further limit condensin function and therefore enhance the $SMC4^{k08819}$/+; $Cap\text{-}H2^{Z3\text{-}0019}$/+ intermediate phenotype. The heterozygous $Mrg15^{j6A3}$ alone does not affect nurse cell polytene unpairing (Figure 3, A–C) since these nurse cells exhibit the same number of FISH spots as wild-type Oregon-R nurse cells (Figure S2). In the sensitized $SMC4^{k08819}$/+; $Cap\text{-}H2^{Z3\text{-}0019}$/+ condensin mutant line, nurse cells exhibit five to eight spots per nucleus (Figure 3, D–F). By contrast, when the $Mrg15^{j6A3}$ mutant was crossed into the double-heterozygous condensin mutant, there was a decrease in the number of spots, indicating a more polytene-like structure (Figure 3, G–I). For each of the three FISH probes, there was a significant difference between the double heterozygote ($Smc4^{k08819}$/+; $Cap\text{-}H2^{Z3\text{-}0019}$/+) and the $Smc4^{k08819}$/+; $Cap\text{-}H2^{Z3\text{-}0019}/Mrg15^{j6A3}$ ($P < 10^{-11}$ for Ubx probe, $P < 10^{-7}$ for 34D probe, $P < 10^{-12}$ for Cap-H2 probe). A deficiency [*Df(3R)BSC741*] that deletes the entire *Mrg15* locus crossed into the sensitized background also decreased the number of FISH spots (Figure 3, J–L). The *Mrg15* deficiency [*Df(3R)BSC741*] alone did not change the number of FISH spots, as compared to wild-type cells, and exhibited no other obvious nurse cell phenotypes (Figure S2). To ensure that this was not a condensin allele-specific interaction, we used a different *Smc4* allele combined with a small deficiency that deletes the *Cap-H2* locus. This condensin $Smc4^{88\text{-}82}$/+; *Df(3R)Exel6195*/+ double heterozygote exhibited seven to nine FISH spots, similar to the $Smc4^{k08819}$/+; $Cap\text{-}H2^{Z3\text{-}0019}$/+ background (Figure S2). By contrast, the $Smc4^{88\text{-}82}$/+; $Df(3R)Exel6195/Mrg15^{j6A3}$ exhibited an average of four to five FISH spots ($P < 10^{-12}$ for Ubx, $P < 10^{-11}$ for 34D, $P < 10^{-5}$ for Cap-H2; Figure S2). This suggests that *Mrg15* genetically interacts with *Smc4* and *Cap-H2* in nurse cells. This interaction is not specific to *Smc4* or *Cap-H2* mutant alleles and therefore is also unlikely to be due to nonspecific genetic background effects in the condensin mutant lines.

RNAi depletion of Mrg15 in nurse cells leads to polytene unpairing defects

To further test the function of *Mrg15* in nurse cell polytene unpairing, we used a TRiP RNAi line capable of expressing an RNA hairpin in the female germline. We used this Mrg15-TRiP in combination with a germline-specific *Matα4-GAL-VP16* driver (Hacker and Perrimon 1998; Januschke *et al.* 2002). First, we confirmed that endogenous Mrg15 protein was expressed in somatic and germline cells of control ovaries from *Matα4-GAL-VP16* transgenic females (Figure 4, A–C) (Kusch *et al.* 2004). Second, we validated RNAi depletion of Mrg15 in ovaries from germline-specific RNAi

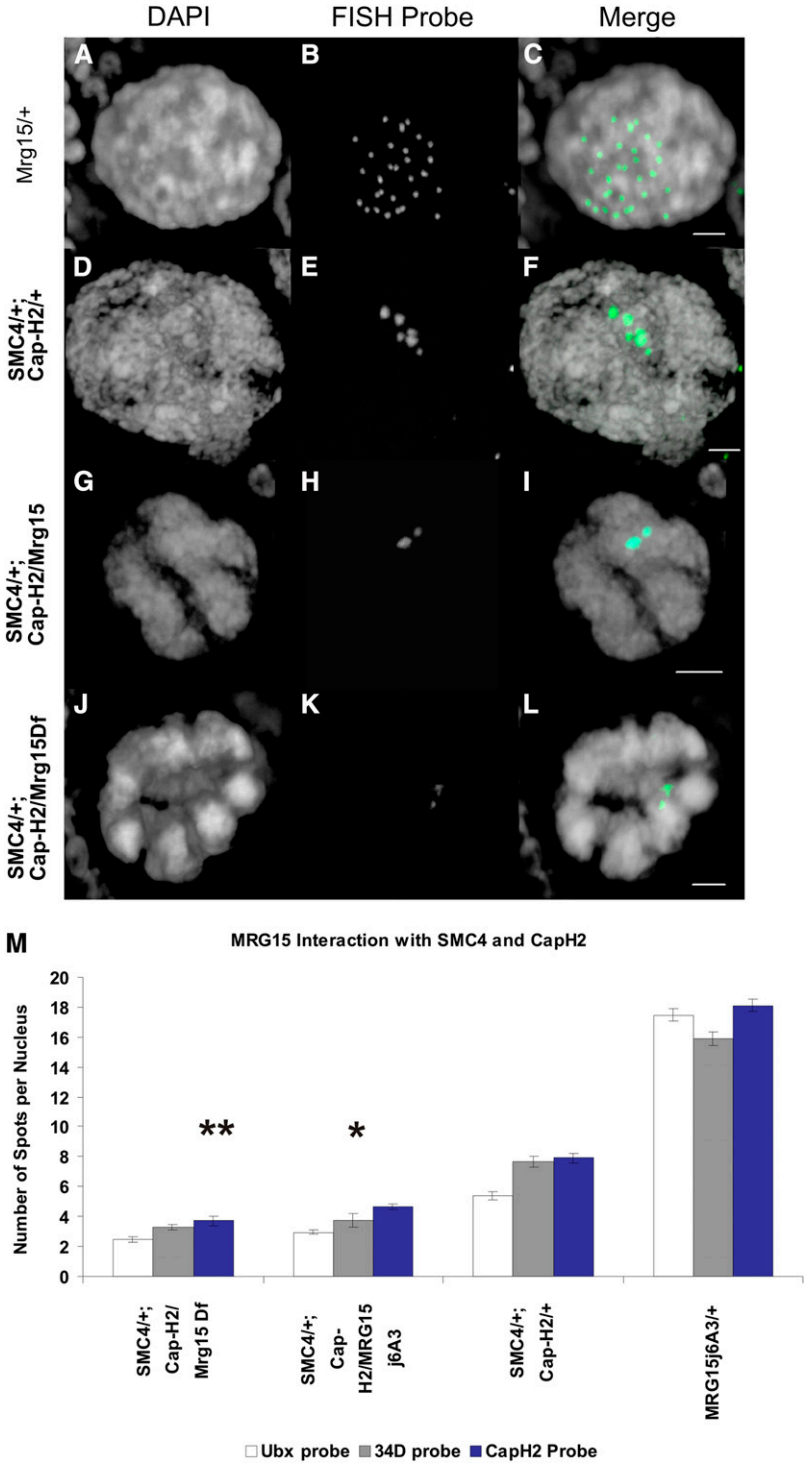

Figure 3 Mrg15 mutants enhance condensin II partial loss of function in ovarian nurse cells. Single ovarian nurse cell nuclei from stage 6/7 egg chambers with the following genotypes: *Mrg15*^{j6A3}/+ (A–C); *SMC4*^{k08819}/+; *Cap-H2*$^{Z3\text{-}0019}$/+ (D–F); *SMC4*^{k08819}/+; *Cap-H2*$^{Z3\text{-}0019}$/*Mrg15*^{j6A3} (G–I); and *SMC4*^{k08819}/+; *Cap-H2*$^{Z3\text{-}0019}$/*Df(3R)BSC741* (J–L). The left column (A, D, G, and J) shows the DAPI channel staining for DNA. The middle column (B, E, H, and K) is the *Ubx* FISH probe. The right column (C, F, I, and L) is a merge of the DAPI in white and the FISH probe in green. Bars, 5 μm. (M) The bars in the graph represent the average number of spots per nucleus for each of three FISH probes: quantitation of FISH spots for *Ubx* is shown in white, 34D is shown in gray, and *Cap-H2* FISH is shown in blue. A single asterisk indicates a significant difference compared to double heterozygote (*SMC4*^{k08819}/+; *Cap-H2*$^{Z3\text{-}0019}$/+) with $P = 1.58 \times 10^{-12}$ (*Ubx*), $P = 3.72 \times 10^{-8}$ (34D), and $P = 3.92 \times 10^{-13}$ (Cap-H2). Two asterisks indicate a significant difference from the double heterozygote (*SMC4*^{k08819}/+; *Cap-H2*$^{Z3\text{-}0019}$/+) with $P = 2.63 \times 10^{-15}$ (Ubx), $P = 6.69 \times 10^{-18}$ (34D), and $P = 1.82 \times 10^{-13}$ (Cap-H2). The genotypes are listed on the *x*-axis. For each of the three probes, the number (*n*) of nuclei scored was as follows: $n \geq 69$ nurse cells for *Mrg15*^{j6A3}/+. $n \geq 59$ for *SMC4*^{k08819}/+; *Cap-H2*$^{Z3\text{-}0019}$. $n \geq 19$ for *SMC4*^{k08819}/+; *Mrg15*^{j6A3}/*Cap-H2*$^{Z3\text{-}0019}$. See Figure S2 and Table S3 for additional supporting data.

(Figure 4, D–F). The first detectable Mrg15 depletion was found in stage 4 nurse cells, and by stage 5/6 protein levels were barely detectable (Figure 4, A and F). Note that stage 5/6 and stage 7 nurse cell DNA has blob-like chromosomes (compare Figure 4A to Figure 4D and Figure 4G to Figure 4J), typical of polytene chromosomes that have failed to unpair (Dej 1999). This suggested that RNAi depletion of endogenous Mrg15 in the ovary could be accomplished.

Because the Gal4 driver is germline specific, the somatic follicle cells that are not affected by the RNAi serve to normalize the Mrg15 protein within control and RNAi-treated egg chambers (Figure 5). We used this to further asses Mrg15 protein levels. A *z*-slice confocal image of a stage 5/6 egg chamber was taken from Figure 4, and pixel intensities were acquired along a single 50- to 60-μm line that crossed exactly two follicle cells (fc1, fc2) and two

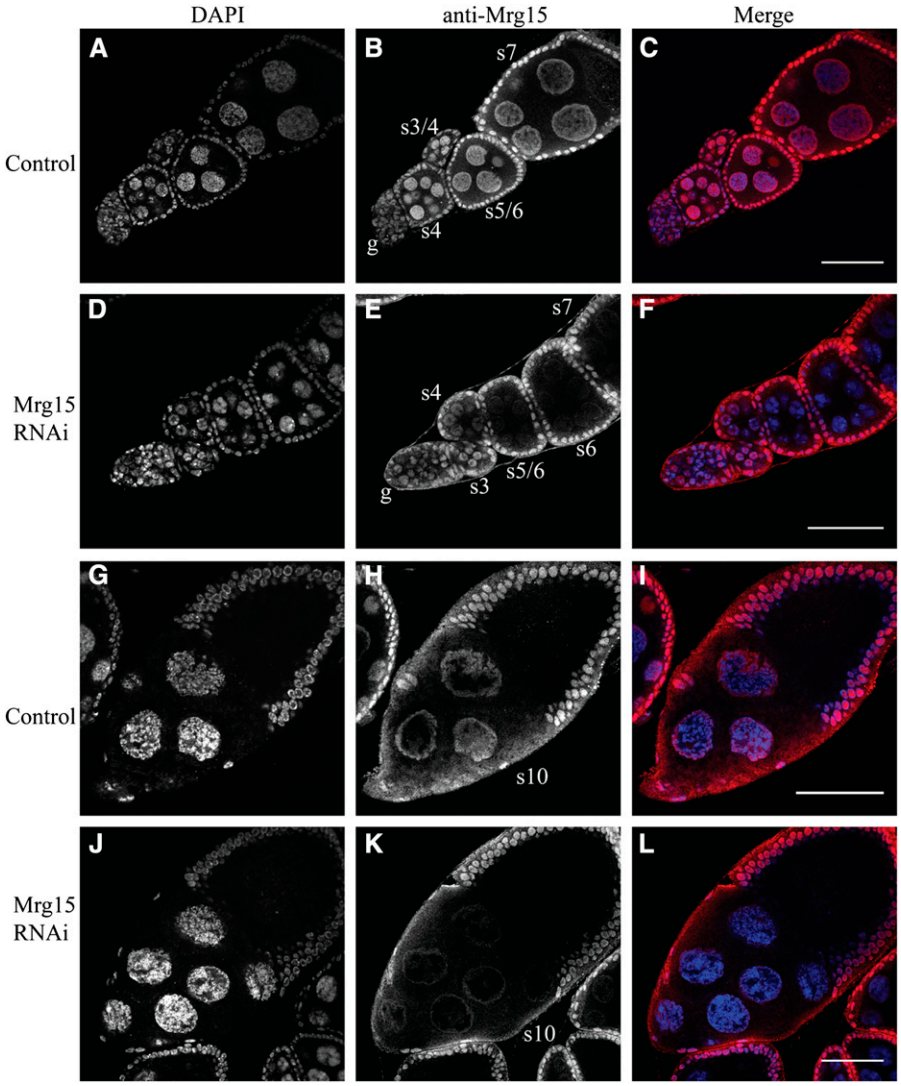

Figure 4 Mrg15 is efficiently depleted by RNAi in the ovary. Egg chambers stained with DAPI and anti-Mrg15 in *Matα4-GAL-VP16* control (A–C) and *Matα4-GAL-VP16, UAS > TRiP:Mrg15* RNAi (D–F). Germarium (g) and stages 3–7 are shown. Stage 10 egg chamber from *Matα4-GAL-VP16* control (G–I) and *Matα4-GAL-VP16, UAS > TRiP:Mrg15* RNAi (J–L). Note the decreases in Mrg15 protein levels in nurse cells but not in follicle cells in stage 4–10 egg chambers. Bar, 50 μm.

nurse cells (nc1, nc2) (Figure 5, A and B and F and G). Intensities along these lines for both DAPI and anti-Mrg15 signal were plotted, and we observed that follicle-cell Mrg15 levels were approximately equal in control and RNAi tissues (Figure 5, C and H). Nuclear-localized Mrg15 protein was also apparent in follicle cells of later stage egg chambers of both control and Mrg15 RNAi ovaries (Figure 4). However, nurse cells from control egg chambers exhibit high levels of Mrg15 while RNAi-expressing nurse cells have vastly reduced Mrg15 staining (Figure 5, A–C and F–H). The position at which nurse cell nuclei (nc1 and nc2) are found within each egg chamber, relative to the Mrg15-positive follicle cells, is noted by the DAPI signal (Figure 5, C and H). Nurse cell DNA in the control egg chamber had the expected unpaired polyploid nuclei with DNA distributed throughout the nucleus (Figure 5, D and E). Nurse cell DNA in the Mrg15 RNAi-depleted egg chamber had nondispersed DNA with blob-like features (Figure 5, I and J).

The level of polytene pairing in nurse cells expressing Mrg15-targeting dsRNA was further evaluated by DNA FISH. In control stage 10 nurse cells, chromosomes were dispersed, as visualized by probes on the X chromosome and chromosome II (Figure 6, A–C). In contrast, 100% ($n > 100$ nuclei) of stage 10 nurse cell nuclei from Mrg15 RNAi-expressing tissue had partially paired or completely paired polytene chromosomes (Figure 6, D–I). The failure to unpair was so severe in nurse cells earlier than stage 6 that it was not possible to count individual FISH spots. In stage 10 egg chambers where individual FISH spots could be counted, we observed that control nurse cells had an average of 42 ± 3 2L-chromosome spots and 40 ± 3 X-chromosome spots (Figure S3). Stage 10 nurse cells from Mrg15 RNAi ovaries had 14 ± 1 2L-chromosome spots and 19 ± 2 X-chromosome spots per nucleus (Figure S3). This represents a significant defect in nurse cell polytene chromosome unpairing (2L probe, $P < 10^{-8}$; X probe, $P < 10^{-6}$; Figure S3). We conclude that Mrg15 protein function is important for normal nurse cell polytene unpairing regardless of condensin status. That both *Mrg15* and condensin gene functions are required to normally drive unpairing of polytene chromosomes in ovarian nurse cells is

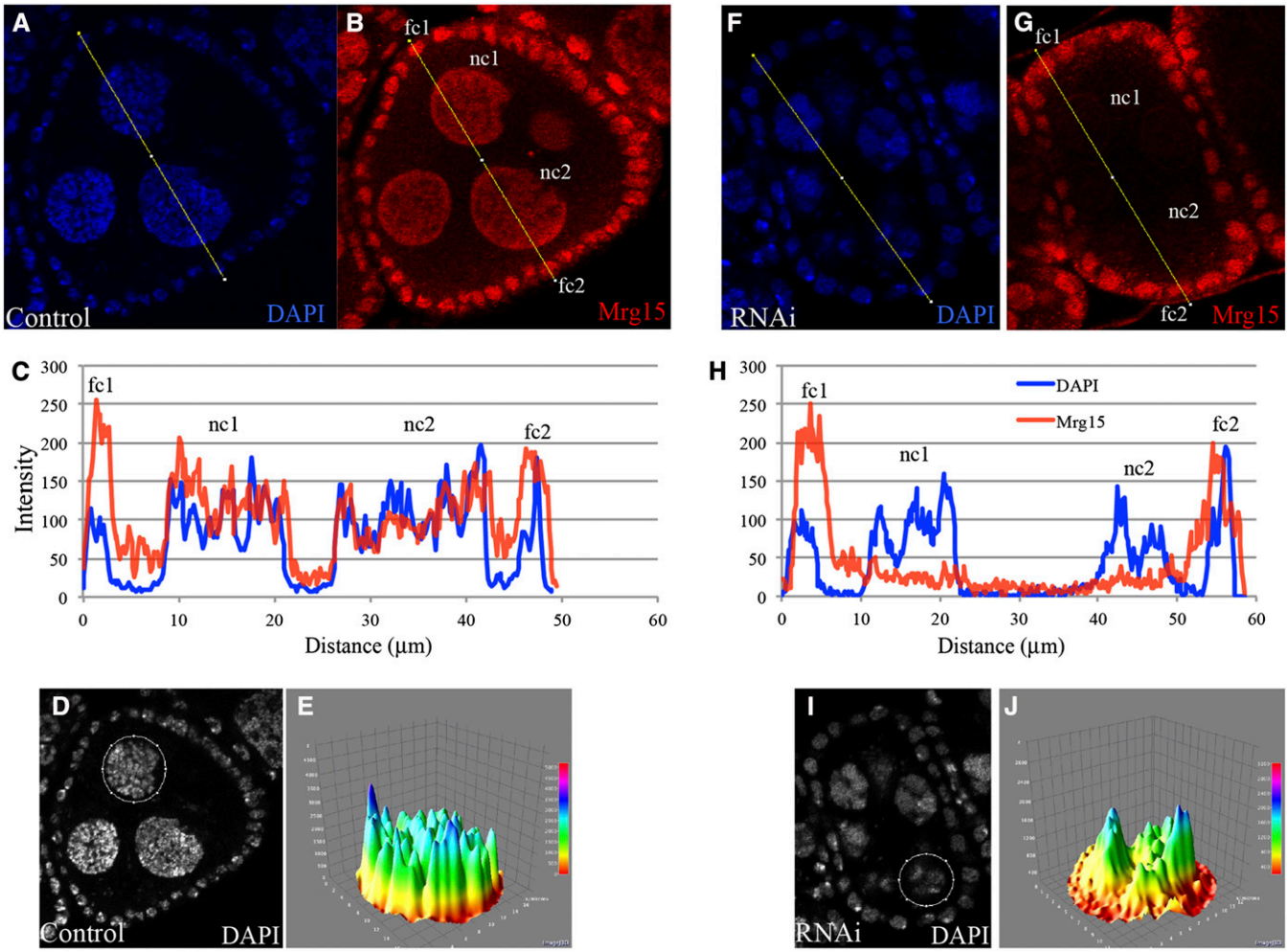

Figure 5 Mrg15 RNAi-depleted nurse cells have altered chromosome organization. Confocal slice of a stage 5/6 egg chamber from control *Matα4-GAL-VP16* stained with DAPI and Mrg15 (A and B). Pixel intensity for DAPI (blue) and Mrg15 (red) was determined along a 50-µm line through the egg chamber. Two follicle cells (fc1, fc2) and two nurse cells (nc1, nc2) were included in the quantitation (C). Single DAPI-stained nucleus from control (D) egg chamber and topographical map of signal intensity showing DNA distribution (E). Confocal slice of a stage 5/6 egg chamber from *Matα4-GAL-VP16*, *TRiP:Mrg15* stained with DAPI and Mrg15 (F and G). Pixel intensity for DAPI (blue) and Mrg15 (red) was determined along a 58-µm line through the egg chamber. Two follicle cells (fc1, fc2) and two nurse cells (nc1, nc2) were included in the quantitation (H). Note that the signal intensity for the follicle-cell nuclei in the *TRiP:Mrg15* sample is comparable to that of the follicle-cell nuclei in the control shown in C. Signal for the Mrg15 protein is vastly diminished in the nurse cells (nc1, nc2). Single DAPI-stained nucleus from the control (I) egg chamber and topographical map of signal intensity showing DNA distribution (J). Note the uneven blob-like distribution of DAPI signal in nurse cells from RNAi egg chambers.

consistent with our observations in the salivary gland where Cap-H2 and Mrg15 are polytene-pairing antagonists (Figure 2).

We note that a previous report has shown that a second-site lethal mutation is also present on the *Mrg15* ^{j6A3} chromosome (Qi *et al.* 2006). Therefore, with experiments where the *Mrg15* ^{j6A3} chromosome was used, we cannot exclude the possibility that this undefined lethal mutation may interact with mutations in *Smc4* and *Cap-H2*. However, because the RNAi depletion of Mrg15 in the salivary gland and in nurse cells (using two different RNAi-transgene systems) gives similar results as the *Mrg15* ^{j6A3} mutation, we suggest that it is highly unlikely that a second-site mutation on this chromosome is responsible for suppression of condensin phenotypes in the salivary gland and enhancement of condensin phenotypes in nurse cells.

Mrg15 antagonizes transvection at Ubx and yellow

Our observations indicated that Mrg15, like Cap-H2, inhibits interchromosomal interactions in polyploid cells, and we wanted to determine whether this was also true in diploid cells. Previously, we showed that in diploid cells *Cap-H2* mutations enhance *trans*-activation (transvection) at the *yellow* and *Ubx* loci, while overexpression can suppress transvection at *Ubx* (Hartl *et al.* 2008a). This *trans*-activation of one mutant allele by the second allele is thought to require extensive physical interactions between the two homologous chromosomes, and chromosomal rearrangements that disrupt diploid homolog pairing also suppress transvection (Lewis 1954). The

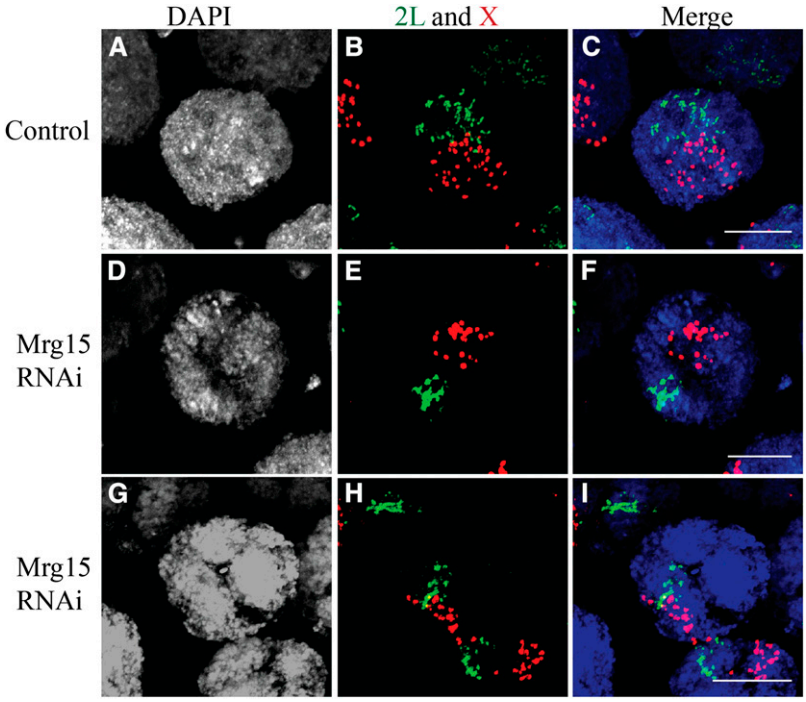

Figure 6 Mrg15 is required for nurse cell polytene unpairing. Confocal projection of a stage 10 single nurse cell nucleus from control *Matα4-GAL-VP16* stained with DAPI (A) and DNA FISH to the 2L (green) and X chromosomes (red) (B) and the merged image (C). Confocal projection of a stage 10 single nurse cell nucleus from *Matα4-GAL-VP16, TRiP:Mrg15* stained with DAPI (D and G) and DNA FISH (E and H) and the merged images (F and I). Note the clustering and fewer FISH spots in the *TRiP:Mrg15* nuclei (E and H) compared to the control in B. Bar, 20 μm. See Figure S3 for additional images and quantitation of FISH spots.

$Ubx^{Cbx\text{-}1}$ Ubx^{1}/++ is a genetic assay for homologous chromosome interactions (Lewis 1954). *Ubx* is normally expressed in nonwing tissues to repress wing-specific gene expression. However, in the $Ubx^{Cbx\text{-}1}$ Ubx^{1}/++ genetic background the *Cbx* enhancer can express *Ubx* in the wing and disrupt development of the ventral side of the wing. This is true despite the fact that the Ubx^{1} mutation, in *cis* with the *Cbx* enhancer, is a *Ubx* null (Figure 7, A and B). Lewis proposed that the *Cbx* enhancer activates, in *trans*, the wild-type copy of *Ubx* on the homologous chromosome (Lewis 1954). If Mrg15 inhibits these *trans*-interactions, like *Cap-H2*, then *Mrg15* mutants are predicted to enhance transvection. We observed that a heterozygous *Mrg15* mutation enhances the $Ubx^{Cbx\text{-}1}$ Ubx^{1} transvection phenotype (Figure 7, C and D) similar to the *Cap-H2* mutant (Hartl *et al.* 2008a). Transvection tests done at the same time with a $Set2^{1}$ loss-of-function mutation in the dSet2 histone methyl transferase did not enhance transvection at *Ubx* (Figure S4). We considered the possibility that Mrg15 is a general repressor of *Ubx* transcription and that this could explain the increase in wing phenotype. One control for this is the transposition of the wild-type allele of *Ubx* to a nonallelic position by a chromosomal rearrangement (BTD), which would be expected to have no effect on the ability of the *Mrg15* mutation to increase *Ubx* expression in the wing. However, if the enhancement of transvection caused by the *Mrg15* mutation is homolog-pairing dependent, then the transposed *Ubx* should not show a phenotype. We found that enhancement of transvection at *Ubx* by a mutation in *Mrg15* does not occur in the translocation background (Figure S4).

Cap-H2 mutations also have been shown to be recessive enhancers of transvection at the *yellow* locus (Hartl *et al.* 2008a). We asked whether a *Mrg15* mutation (alone or in combination with *Cap-H2* mutations) could also modify the $y^{1\#8}/y^{82f29}$-transvecting alleles. We scored all female progeny from different crosses into four classes based on darkly pigmented abdominal stripes (see *Materials and Methods* and Figure 8), as previously described (Hartl *et al.* 2008a). We observed that ~20% of all $y^{1\#8}/y^{82f29}$; $Mrg15^{j6A3}$/+ females were darkly pigmented (class 3 and 4), and this was not significantly different from $y^{1\#8}/y^{82f29}$; $Cap\text{-}H2^{Z3\text{-}0019}$/+, and $y^{1\#8}/y^{82f29}$; *Df(3R)Exel6195*/+ females (Figure 8). Thus, these three heterozygous controls do not differ from each other in the proportion of darkly pigmented females (pigmentation class 3 and 4). By contrast, we observed that 60–65% of all $y^{1\#8}/y^{82f29}$;$Cap\text{-}H2^{Z3\text{-}0019}/Mrg15^{j6A3}$ and $y^{1\#8}/y^{82f29}$;*Df(3R)Exel6195*/$Mrg15^{j6A3}$ females were darkly pigmented (Figure 8). This represents a significant enhancement of transvection at the *yellow* locus when both *Cap-H2* and *Mrg15* are heterozygous. Because *Mrg15* is an essential gene (Kusch *et al.* 2004), it is not possible to test homozygous effects on transvection. Furthermore, because the $Mrg15^{j6A3}$ chromosome has previously been shown to contain a second lethal mutation (Qi *et al.* 2006), these studies were done in a line where $Mrg15^{j6A3}$ was allowed to recombine over seven generations in a w^{1118} background. These data suggest that *Mrg15*, like *Cap-H2*, normally functions to inhibit transvection at *Ubx* and *yellow* and/or interacts with *Cap-H2* to regulate the expression of *Ubx* and *yellow*. However, we cannot exclude the possibility that *Mrg15* could alter expression of both the *Ubx* and *yellow* genes in a manner that is independent of chromosomal interactions leading to transvection.

Cap-H2 levels on chromatin are dependent on Mrg15 levels

The physical interaction between Cap-H2 and Mrg15 maps to the Mrg domain that is not overlapping with the chromodomain (Figure 1). These results suggest that the MRG domain

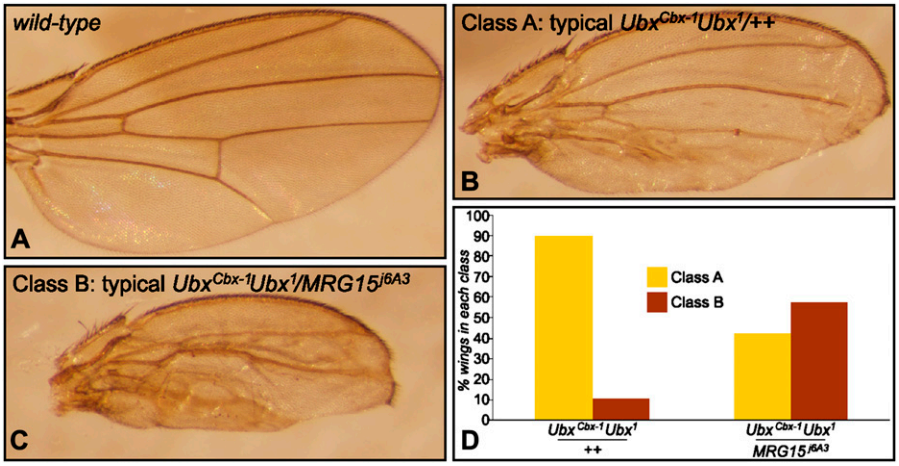

Figure 7 Mrg15 antagonizes transvection at *Ubx*. (A) Wild-type wing from Oregon-R. (B) Wing of class A typical of $Ubx^{Cbx\text{-}1}$ Ubx^{1}/++. (C) Wing of class B typical of $Ubx^{Cbx\text{-}1}$ Ubx^{1}/$Mrg15^{j6A3}$. (D) Quantification of phenotypic classes for $Ubx^{Cbx\text{-}1}$ Ubx^{1}/++ and $Ubx^{Cbx\text{-}1}$ Ubx^{1}/$Mrg15^{j6A3}$. $n > 50$ for both genotypes. $P < 10^{-3}$ for either class using the χ-square test. See Figure S3 for additional supporting data.

of Mrg15 could act as a region to bind to Cap-H2, while the chromodomain serves to bind Mrg15 to chromatin; therefore, Mrg15 may serve as a tether to recruit the Cap-H2 protein to chromatin. To test this possibility, we measured levels of Cap-H2 bound to chromatin in cultured *Drosophila* S2 cells as previously done for Cap-H2 chromatin-fractionation studies (Buster *et al.* 2013). We compared control RNAi chromatin-bound Cap-H2 levels in S2 cells to those depleted of Mrg15 by RNAi. To accomplish this, pMT-Cap-H2-EGFP or pMT-Cap-H2-V5 were transfected into S2 cells, and we used anti-GFP or anti-V5 antibody to determine levels of Cap-H2 in the whole-cell lysate, cytosolic, soluble nuclear, and chromatin-bound fractions in control RNAi-treated cells and in cells depleted by RNAi of Mrg15. First, whole-cell lysates show a single major band when probed with anti-Mrg15, anti-V5, or anti-lamin (Figure 9 and Figure S5). Treatment of cells with dsRNA directed to Mrg15 sequences depleted endogenous Mrg15 protein by ~75% relative to extracts from dsRNA to a control sequence within the pBlueScript SK plasmid (Figure S5), and this level of depletion was consistent in four biological replicates. Upon cell fractionation followed by immunoblot analysis, Cap-H2 chromatin-bound levels were normalized to lamin chromatin-bound levels for each treatment (mock RNAi control and Mrg15 RNAi); the same calculation was performed for whole-cell lysate levels of Cap-H2 and lamin in each treatment [*Materials and Methods* and as previously described (Buster *et al.* 2013)]. Subsequently, the chromatin-bound Cap-H2/lamin ratio was divided by the Cap-H2/lamin whole-cell lysate ratio to calculate chromatin-bound enrichment. We then compared the chromatin-bound enrichment value between the control RNAi and Mrg15 RNAi treatments. We found that Cap-H2-EGFP (or Cap-H2-V5) bound to chromatin in Mrg15 RNAi-treated cells was reduced by >50% ($P < 0.005$) compared to that in cells treated with a control RNAi (Figure 9). By normalizing to whole-cell lysate lamin levels, we also determined that levels of Cap-H2 expression did not significantly differ between control RNAi and Mrg15 RNAi treatments. These data suggest that in S2 cells Mrg15 protein facilitates Cap-H2 tethering to chromatin. Although anti-Cap-H2 antibodies have been reported, we found that this reagent is not of sufficient quality to detect endogenous protein in whole-cell lysates, and thus the effects of Mrg15 on endogenous chromatin-bound Cap-H2 could not be ascertained.

Mrg15 and Cap-H2 are required to maintain chromosome compaction and function as antipairing factors in cultured cells

The loss of condensin II activity results in chromosome length increases in interphase polyploid cells, coincident with a failure to unpair polytene chromosomes (Bauer *et al.* 2012). This suggests that condensins are necessary for maintaining some level of interphase chromosome compaction. In addition, Cap-H2, Cap-D3, and Smc2 condensin subunits have recently been identified as heterochromatin antipairing factors in cultured Kc_{167} cells (Joyce *et al.* 2012). To determine whether the Cap-H2 axial compaction and antipairing functions was Mrg15 dependent, we used 3D DNA FISH in Kc cells to measure chromosome compaction and homolog pairing. Note that because homologs are normally paired at high frequency in most *Drosophila* cells, including Kc cells, each unique FISH probe is expected to give only one spot in most nuclei (Figure 10, A–F, arrow). In some cells two or more FISH spots can be seen for each of the probes (Figure 10, A–F, arrowhead), and multiple probes on the same chromosome allow for an indirect measure of axial compaction (Figure 10, G and H). Using three different probes on the X chromosome (all in euchromatin), we found that RNAi depletion of Mrg15 (validated by immunoblots; Figure S5) gave a slight decrease in the average number of FISH spots per nucleus, relative to a control RNAi treatment (Figure 10I). Overexpression of Cap-H2, however, resulted in a dramatic increase in the average number of FISH foci per nucleus (Figure 10I). Cap-H2 overexpression also led to a decrease in the proportion of nuclei with paired homologs from 80% of cells with paired homologs in control cells compared to 35% ($P < 0.005$) paired in Cap-H2-overexpressing cells (Figure 10J). This suggests that Cap-H2 overexpression is sufficient to drive unpairing of homologs, consistent with its previously reported antipairing function. By contrast, overexpression of Cap-H2 in combination with

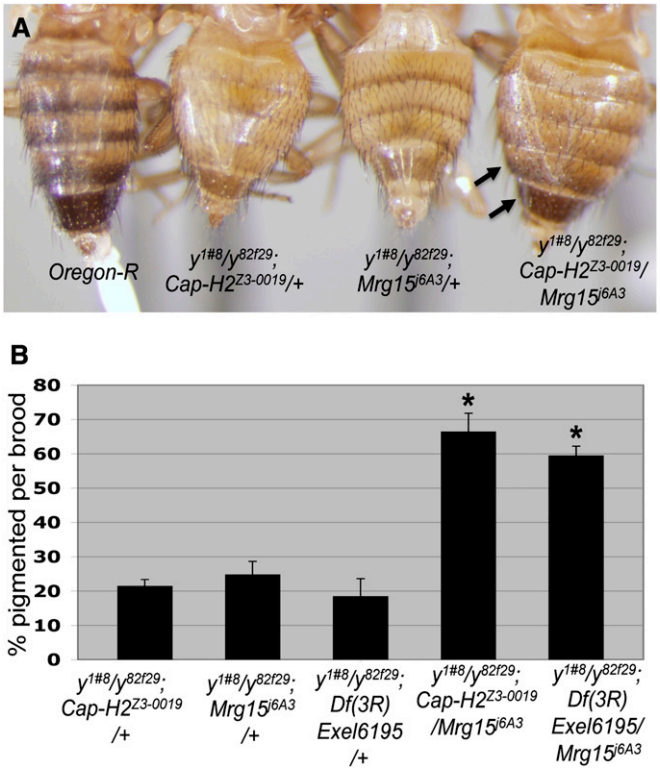

Figure 8 Mrg15 cooperates with Cap-H2 to antagonize transvection at *yellow*. (A) Similarly aged females with the following genotypes from left to right: *Oregon-R*, $y^{1\#8}/y^{82f29}$; *Cap-H2*$^{Z3\text{-}0019}$/+, $y^{1\#8}/y^{82f29}$;*Mrg15*^{j6A3}/+ and $y^{1\#8}/y^{82f29}$; *Cap-H2*$^{Z3\text{-}0019}$/*Mrg15*^{j6A3}. Arrows point to darkly pigmented posterior stripes. (B) Percentage of all female progeny exhibiting darkly pigmented posterior stripes per brood for the following genotypes left to right: $y^{1\#8}/y^{82f29}$; *Cap-H2*$^{Z3\text{-}0019}$/+ (n = 53), $y^{1\#8}/y^{82f29}$;*Mrg15*^{j6A3}/+ (n = 77), $y^{1\#8}/y^{82f29}$;*Df(3R)Exel6195*/+ (n = 45), $y^{1\#8}/y^{82f29}$; *Cap-H2*$^{Z3\text{-}0019}$/*Mrg15*^{j6A3} (n = 96), and $y^{1\#8}/y^{82f29}$;*Df(3R)Exel6195/Mrg15*^{j6A3} (n = 91). Asterisks denote $P < 0.001$, two-tailed t-test assuming unequal variance.

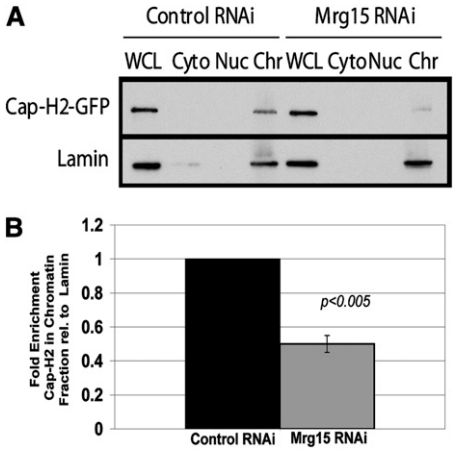

Figure 9 Chromatin-bound Cap-H2 is partially dependent on Mrg15 levels. S2 cells transfected with pMT-Cap-H2-EGFP: (A) Cells were treated with control RNAi and RNAi targeting Mrg15. Cells expressing Cap-H2-EGFP were fractionated, and extracts were immunoblotted with anti-GFP and anti-Lamin. Anti-Mrg15 immunoblots were used to confirm RNAi depletion of Mrg15 (see Figure S5). Each lane represents 20 μg of whole-cell lysates (WCL), cytosolic (Cyto), soluble nuclear (Nuc), and chromatin bound (Chr). (B) The fold enrichment of Cap-H2-EGFP in the chromatin fraction was calculated from four biological replicates as described in *Materials and Methods* ($P < 0.005$, two tailed t-test assuming unequal variance). Control RNAi is shown with the solid bar and Mrg15 RNAi is shown with the shaded bar. (See Figure S5 for supporting data.)

RNAi depletion of Mrg15 both rescued the average number of FISH spots per nucleus and increased the percentage of nuclei with paired homologs to 59% ($P < 0.04$) (Figure 10, I and J).

To measure axial compaction, we used pairs of probes on the same chromosome. Using three different probes on the X chromosome and two different probes on the second chromosome (all in euchromatin), we found that RNAi depletion of Cap-H2 or Mrg15 increased the 3D distance between these sequences by ~0.2 μm (17–23%) for each pairwise probe distance, when compared to a control RNAi treatment ($P < 0.03$, Figure 10K). RNAi depletion of both Cap-H2 and Mrg15 resulted in an even greater increase in distance between probes, ranging from 0.31 to 0.51 μm (24–63%) longer than the control RNAi (**$P < 0.03$; Figure 10K). By contrast, overexpression of *Cap-H2* led to axial shortening of chromosomes by 0.18–0.41 μm (20–61%), relative to control cells (***$P < 10^{-4}$; Figure 10K). This Cap-H2-induced axial shortening was almost completely rescued by RNAi depletion of Mrg15, where probe distances differed by 0.03–0.04 μm compared to the control RNAi-treated cells ($P = 0.6$; Figure 10K).

Although our previous studies were on nonmitotic polyploid cells, here we considered the possibility that altering the Cap-H2 levels could change the number of cells in mitosis, thus skewing chromosome compaction measurements. To determine whether the fraction of cells in mitosis was altered by depletion or overexpression of Cap-H2, we stained cells with antiphospho-histone H3. We found that 0.01% of control cells were phospho-H3 positive, while 0.014% of Cap-H2 RNAi cells and 0.01% of Cap-H2 overexpression cells were phospho-H3 positive ($n > 395$ cells for each treatment, $P > 0.2$). These observations are consistent with previous findings that altering Cap-H2 levels results in changes in interphase chromosome length in *Drosophila* (Bauer *et al.* 2012). Mrg15 RNAi depletion did not lead to mitotic arrest or delay as 0.009% of cells were phospho-H3 positive, while 0.01% of control RNAi-treated cells were phospho-H3 positive ($n > 600$ cells, $P = 0.21$). In addition, nuclear size for cells after any RNAi treatment or Cap-H2 overexpression was not significantly different from control RNAi-treated cells. We conclude that both Cap-H2 and Mrg15 are required to maintain interphase chromosome compaction in cultured Kc cells, consistent with a condensin II axial shortening function (Shintomi and Hirano 2011; Bauer *et al.* 2012).

Discussion

A previously reported large-scale yeast two-hybrid screen found that *Drosophila* Cap-H2 and Mrg15 proteins interact (Giot *et al.* 2003). Here, we have replicated this result and show that Cap-H2 interacts with the MRG domain of Mrg15

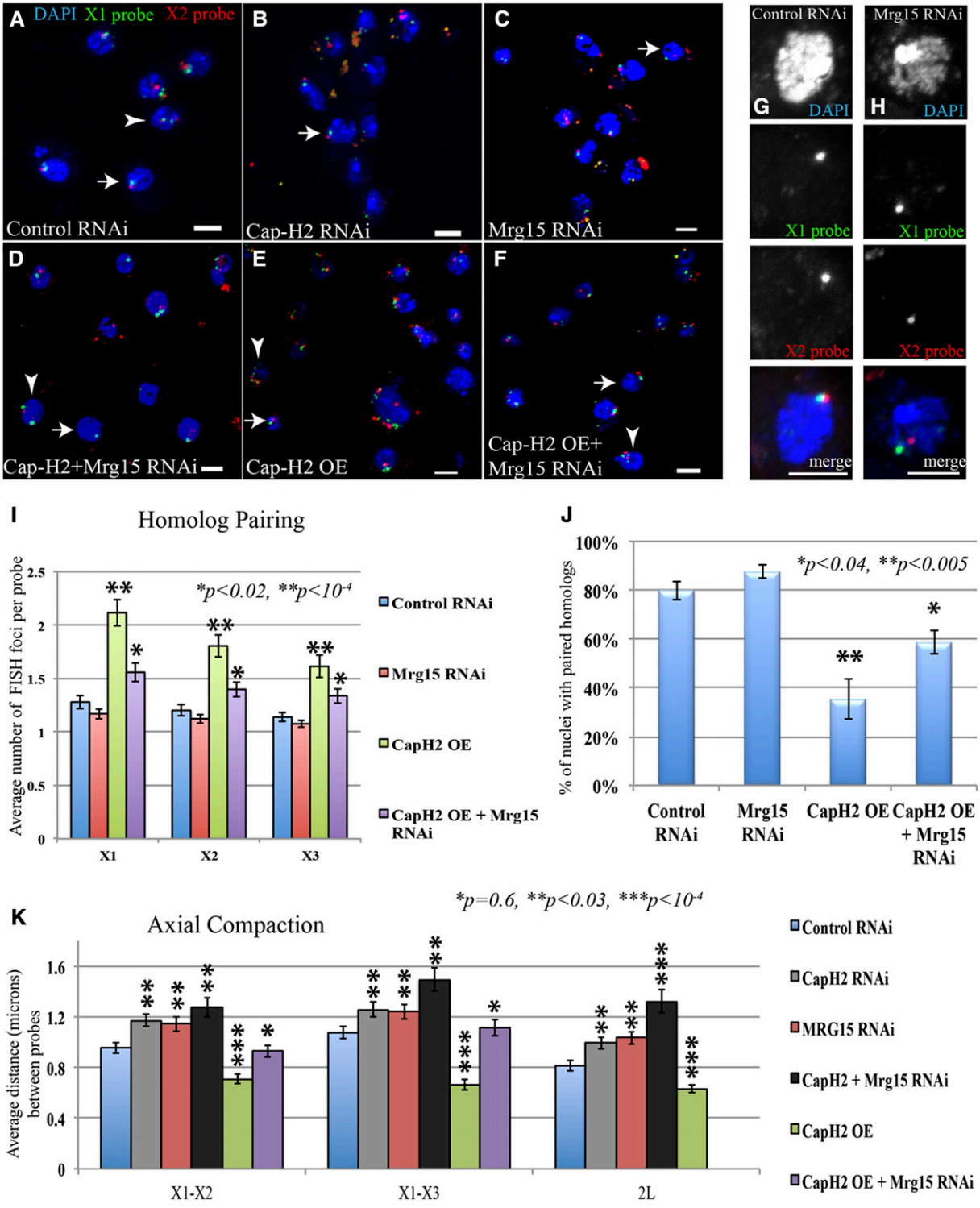

Figure 10 Cap-H2 and Mrg15 are required to maintain chromosome length and control axial compaction. (A–F) Cultured Kc cell nuclei stained with DAPI (blue), X-chromosome probe 1 (X1 probe, green), and X-chromosome probe 2 (X2 probe, red). Arrows indicate nuclei with a single FISH spot for each probe showing paired homologs. Arrowheads indicate nuclei with multiple spots of unpaired homologs. (A) Cells treated with control RNAi. (B) Cells treated with RNAi targeting Cap-H2. (C) Cells treated with RNAi targeting Mrg15. (D) Cells treated with RNAi targeting both Cap-H2 and Mrg15. (E) Cells with Cap-H2 overexpression (OE) from pMT-Cap-H2. (F) Cells with Cap-H2 overexpression plus RNAi targeting Mrg15. (G) Single nucleus of control RNAi and (H) Mrg15 RNAi probed with two different probes on the X chromosome. (I) The average number of FISH spots per probe per cell is indicated as a measure of homolog pairing. Spots were counted as one spot if they were merged or their centers were <0.2 μm apart. (J) The proportion of nuclei with paired homologs is shown. (K) Pairwise distances were measured in 3D image reconstructions for three different FISH probe pairs: X1–X2 (~2.05 Mb apart), X1–X3 (~3.6 Mb apart) probes were on the X chromosomes, and 2L (~2 Mb apart) probes were on the left arm of the second

while the chromodomain is not sufficient for an interaction with Cap-H2 (Figure 1A). Immunoprecipitation with S2 cell extracts further supports this interaction (Figure 1). In ovarian nurse cells, where condensin is normally required for polytene unpairing, two different *Mrg15* heterozygous mutants enhanced condensin mutant chromosome unpairing defects (Figure 3). Similarly, *Mrg15* RNAi knockdown or a decrease in its gene dosage by 50% in the salivary glands suppressed *Cap-H2*-induced polytene dispersal (Figure 2). Mutations in *Mrg15* showed similar enhancement of transvection at the *Ubx* locus and interactions with Cap-H2 mutations to enhance transvection at the *yellow* locus (Figure 7 and Figure 8). We cannot exclude the possibility that both Mrg15 and Cap-H2 proteins cooperate to directly regulate *Ubx* and *yellow* transcription, as opposed to productive homolog pairing that leads to transvection. However, our observations reported here and previous studies in polyploid, diploid, and male meiotic chromosomes suggesting that Cap-H2 is required for chromosome unpairing (Hartl *et al.* 2008a,b) support a model in which Cap-H2 and Mrg15 antagonize transvection by inhibiting *trans*-interactions. That Cap-H2 provides a homolog antipairing activity has recently been shown for euchromatic and heterochromatic sequences in cultured *Drosophila* cells (Joyce *et al.* 2012; Buster *et al.* 2013) also suggests a more direct function in antagonizing transvection. Interestingly, the Mrg15 homolog in *Caenorhabditis elegans* (Mrg-1) has also been suggested to antagonize ectopic pairing in meiosis (Dombecki *et al.* 2011). Additionally, using cellular fractionation we observed that RNAi depletion of endogenous Mrg15 protein in S2 cells results in an approximately twofold decrease of chromatin-bound Cap-H2 protein (Figure 9). RNAi depletion of Mrg15 in cultured Kc cells leads to axial lengthening of interphase chromosomes (Figure 10K), consistent with a chromatin compaction function thought to be provided by condensins (Shintomi and Hirano 2011; Bauer *et al.* 2012). Importantly, axial compaction driven by overexpression of Cap-H2 can be suppressed by RNAi depletion of Mrg15 (Figure 10K). This suggests that interphase Cap-H2-mediated compaction in polyploid cells *in vivo* and in cultured cells is Mrg15 dependent.

These data raise the possibility that a protein–protein interaction between Cap-H2 and Mrg15 is important for Cap-H2 activity *in vivo*. Because chromatin-bound Cap-H2 levels are partially Mrg15 dependent (Figure 9), and because Cap-H2 interacts with the MRG domain, we speculate that this interaction allows the chromodomain of Mrg15 to recruit Cap-H2 to chromatin. These data do not exclude the possibility that Mrg15 also functions to regulate Cap-H2 activity in a manner that is independent of a possible chromatin-tethering role. A model in which Mrg15 allows tethering or enrichment of Cap-H2 to chromatin through direct protein–protein interactions with the MRG domain of Mrg15 is attractive because the Mrg15 chromodomain is known to bind to methylated histones (Kusch *et al.* 2004; Joshi and Struhl 2005; Zhang *et al.* 2006; Filion *et al.* 2010; Moore *et al.* 2010). We speculate that such a mechanism could be utilized in interphase cells to recruit condensin activity to specific genomic regions marked by histone methylation. This idea is similar to what has been proposed for the Cap-D3 condensin II subunit that interacts with pRB, and pRB is proposed to tether Cap-D3 to centromeric chromatin to effect compaction during mitosis (Longworth *et al.* 2008; Manning *et al.* 2010). Currently, it is not clear if histone methylation or histone methyl transferases, such as Set2, play any role in Cap-H2 tethering to chromatin (Figure S2 and Figure S3). Future studies that systematically examine histone methyl transferases will be necessary.

Mrg15 can also associate with chromatin through interactions with the Tip60 complex (Kusch *et al.* 2004) and potentially provide an indirect mechanism of recruiting condensins to chromatin. We tested *reptin* and *Tip60* mutants in both the salivary glands and the ovary. RNAi to *reptin* led to high larval lethality, and those few larvae that were alive had very small salivary glands (data not shown). In the ovary, two different *reptin* mutants showed similar levels of enhancement when crossed to the $Smc4^{k08819}/+$; $Cap\text{-}H2^{Z3\text{-}0019}/+$ double heterozygote (Figure S2, top). The level of enhancement was equal if not greater than that of the *Mrg15* mutants (Figure S2 and Table S3). This is consistent with the idea of the two proteins, reptin and Mrg15, working in the same complex. In *Drosophila*, Mrg15 and reptin proteins have been copurified and also show similar genetic interactions in position-effect variegation (Kusch *et al.* 2004; Qi *et al.* 2006). Interestingly, the reptin protein and its binding partner pontin, also known as RVB2/RVB1, may have DNA/RNA-binding functions and participate in a variety of chromatin-remodeling complexes (Jha and Dutta 2009), further linking condensins and Mrg15 to chromatin- and histone-modifying activities. When we performed RNAi to *Tip60* in conjunction with *Cap-H2* overexpression in the salivary glands, there was no significant suppression observed (Figure S1). However, when a *Tip60* mutant ("Tip60G," $Tip60^{GG01739}$; Table S3) was crossed into the $SMC4^{k08819}/+$; $Cap\text{-}H2^{Z3\text{-}0019}/+$ double heterozygote, we did observe significant suppression of the polytene unpairing defect (Figure S2, top). This means that the ovarian nurse cells became less polytene and looked more like wild type, which is contrary to the enhancing effect of *Mrg15* and *reptin* mutants (Figure 3 and Figure S2). A different transposon insertion at *Tip60* ("Tip60E," $Tip60^{e02395}$) did not modify the condensin polytene nurse cell phenotype (Figure S2, top). Although

chromosome (see *Materials and Methods* and Table S4). Significance levels were calculated by *t*-test, assuming equal variance in Microsoft Excel (*P = 0.6, **$P < 0.03$, and ***$P < 10^{-4}$). All *P*-values are calculated relative to control RNAi samples. Table S4 contains further details including number of nuclei measured, average distances, standard error, and *P*-values. Bars, 5 μm.

intriguing, the exact role of Tip60 in polytene structure and Cap-H2 activity is not clear, and further studies will be required to determine whether Tip60 directly contributes to these observed phenotypes.

In both mammalian and *Drosophila* cells, the retinoblastoma (Rb) transcriptional repressor has been shown to directly interact with the Cap-D3 condensin II subunit (Longworth *et al.* 2008). The Rb protein also forms a complex with Mrg15, and Mrg15 blocks the Rb transcriptional repressor activity (Leung *et al.* 2001). Together, these observations suggest that chromatin factors, such as Mrg15 and Rb, facilitate condensin activities *in vivo*, perhaps by recruitment of condensins to specific genomic regions. The existence of these protein complexes also raises the interesting possibilities that, in proliferating cells, condensins interact with chromatin-remodeling complexes to coordinate cell-cycle progression and/or transcriptional regulation to changes in global chromosome compaction states. Coordination of chromosome organization, condensation, and transcriptional "bookmarking" is likely to be important for maintenance of epigenetic expression states, and local inactivation of condensin activity has been posited to serve such a bookmarking function (Xing *et al.* 2005, 2008). Our observations that mutations in *Cap-H2* and *Mrg15* result in enhancement of transvection at two different loci is consistent with the idea that condensin inactivation may be required for inheritance of active transcriptional states, possibly by regulating *trans*-interactions such as those observed at transvecting loci. Recently, it has been shown that *trans*-splicing of mRNA can occur in *Drosophila* and that homolog-pairing status was proposed to play a role in facilitating *trans*-splicing between paired alleles (McManus *et al.* 2010). Interestingly, in mammalian cells alternative RNA splicing is thought to be influenced by histone H3K36 methylation of intron/exon boundaries (Luco *et al.* 2010, 2011). It will be of great interest to determine whether Mrg15 and Cap-H2 modulation of allelic interactions use histone methylation patterns to also regulate pre-mRNA *trans*-splicing in *Drosophila*.

That interphase chromosome length may be actively regulated is a novel observation (Figure 10K) (Bauer *et al.* 2012). Recent reports have proposed that local and global condensin-mediated chromatin compaction is important for mammalian T-cell quiescence and erythroid maturation (Xu *et al.* 2006; Rawlings *et al.* 2011). Thus, it is intriguing that both Cap-H2 and Mrg15 are necessary for interphase chromosome length maintenance in *Drosophila* cells (Figure 10K), as the Cap-H2 mouse homolog has been shown to be required for chromatin compaction necessary for maintenance of T-cell quiescence (Rawlings *et al.* 2011). Whether Cap-H2, and its interaction with Mrg15, have a function in coordinating global interphase chromosome structure with transcriptional processes remains to be determined. It is also unclear whether histone methylation states serve as docking sites for the Mrg15–Cap–H2 complexes or whether other factors serve to recruit Cap-H2 activity to specific genomic regions. It will be of interest to reveal genome-wide condensin localization patterns and how these relate to local functions such as interphase chromatin compaction and gene activity, propensity for transvection, RNA *trans*-splicing, and general chromatin states.

Acknowledgments

We thank all of the Bosco lab members for helpful discussion and are grateful for the essential community resources provided by FlyBase, the University of California at Santa Cruz Genome Browser, the Bloomington Stock Center, the Vienna Drosophila RNAi Center, the Harvard TRiP collection, the University of Iowa Developmental Studies Hybridoma Bank for antibodies, and the Drosophila Genomics Resource Center for cell lines. We thank the anonymous reviewer for extensive comments making this third revision possible and M. Heck, J. L. Workman, and T. Kusch for antibodies. This work was funded by National Institutes of Health grant R01GM69462 to G.B.

Literature Cited

Bateman, J. R., E. Larschan, R. D'Souza, L. S. Marshall, K. E. Dempsey *et al.*, 2012 A genome-wide screen identifies genes that affect somatic homolog pairing in *Drosophila*. G3 2: 731–740.

Bauer, C. R., T. A. Hartl, and G. Bosco, 2012 Condensin II promotes the formation of chromosome territories by inducing axial compaction of polyploid interphase chromosomes. PLoS Genet. 8: e1002873.

Bazile, F., J. St-Pierre, and D. D'Amours, 2010 Three-step model for condensin activation during mitotic chromosome condensation. Cell Cycle 9: 3243–3255.

Belmont, A. S., 2006 Mitotic chromosome structure and condensation. Curr. Opin. Cell Biol. 18: 632–638.

Bertram, M. J., and O. M. Pereira-Smith, 2001 Conservation of the MORF4 related gene family: identification of a new chromo domain subfamily and novel protein motif. Gene 266: 111–121.

Bertram, M. J., N. G. Berube, X. Hang-Swanson, Q. Ran, J. K. Leung *et al.*, 1999 Identification of a gene that reverses the immortal phenotype of a subset of cells and is a member of a novel family of transcription factor-like genes. Mol. Cell. Biol. 19: 1479–1485.

Bosco, G., 2012 Chromosome pairing: a hidden treasure no more. PLoS Genet. 8: e1002737.

Buster, D. W., S. G. Daniel, H. Q. Nguyen, S. L. Windler, L. C. Skwarek *et al.*, 2013 SCFSlimb ubiquitin ligase suppresses condensin II-mediated nuclear reorganization by degrading Cap-H2. J. Cell Biol. 201: 49–63.

Chen, M., K. Tominaga, and O. M. Pereira-Smith, 2010 Emerging role of the MORF/MRG gene family in various biological processes, including aging. Ann. N. Y. Acad. Sci. 1197: 134–141.

Cobbe, N., E. Savvidou, and M. M. Heck, 2006 Diverse mitotic and interphase functions of condensins in Drosophila. Genetics 172: 991–1008.

Cremer, T., and C. Cremer, 2006 Rise, fall and resurrection of chromosome territories: a historical perspective. Part II. Fall and resurrection of chromosome territories during the 1950s to 1980s. Part III. Chromosome territories and the functional nuclear architecture: experiments and models from the 1990s to the present. Eur. J. Histochem. 50: 223–272.

Cuylen, S., and C. H. Haering, 2011 Deciphering condensin action during chromosome segregation. Trends Cell Biol. 21: 552–559.

Dej, K. J., 1999 The structure and function of the nurse cell chromosomes during oogenesis in *Drosophila melanogaster*, Ph.D. Dissertation, The Johns Hopkins Unversity, Baltimore.

Dej, K. J., and A. C. Spradling, 1999 The endocycle controls nurse cell polytene chromosome structure during Drosophila oogenesis. Development 126: 293–303.

Dombecki, C. R., A. C. Chiang, H. J. Kang, C. Bilgir, N. A. Stefanski *et al.*, 2011 The chromodomain protein MRG-1 facilitates SC-independent homologous pairing during meiosis in Caenorhabditis elegans. Dev. Cell 21: 1092–1103.

Dundr, M., 2012 Nuclear bodies: multifunctional companions of the genome. Curr. Opin. Cell Biol. 24: 415–422.

Filion, G. J., J. G. van Bemmel, U. Braunschweig, W. Talhout, J. Kind *et al.*, 2010 Systematic protein location mapping reveals five principal chromatin types in Drosophila cells. Cell 143: 212–224.

Geyer, P. K., M. M. Green, and V. G. Corces, 1990 Tissue-specific transcriptional enhancers may act in trans on the gene located in the homologous chromosome: the molecular basis of transvection in Drosophila. EMBO J. 9: 2247–2256.

Giot, L., J. S. Bader, C. Brouwer, A. Chaudhuri, B. Kuang *et al.*, 2003 A protein interaction map of Drosophila melanogaster. Science 302: 1727–1736.

Green, L. C., P. Kalitsis, T. M. Chang, M. Cipetic, J. H. Kim *et al.*, 2012 Contrasting roles of condensin I and condensin II in mitotic chromosome formation. J. Cell Sci. 125: 1591–1604.

Hacker, U., and N. Perrimon, 1998 DRhoGEF2 encodes a member of the Dbl family of oncogenes and controls cell shape changes during gastrulation in Drosophila. Genes Dev. 12: 274–284.

Hartl, T. A., H. F. Smith, and G. Bosco, 2008a Chromosome alignment and transvection are antagonized by condensin II. Science 322: 1384–1387.

Hartl, T. A., S. J. Sweeney, P. J. Knepler, and G. Bosco, 2008b Condensin II resolves chromosomal associations to enable anaphase I segregation in Drosophila male meiosis. PLoS Genet. 4: e1000228.

Henikoff, S., and T. D. Dreesen, 1989 Trans-inactivation of the Drosophila brown gene: evidence for transcriptional repression and somatic pairing dependence. Proc. Natl. Acad. Sci. USA 86: 6704–6708.

Hirano, M., and T. Hirano, 2006 Opening closed arms: long-distance activation of SMC ATPase by hinge-DNA interactions. Mol. Cell 21: 175–186.

Hirano, T., 2006 At the heart of the chromosome: SMC proteins in action. Nat. Rev. Mol. Cell Biol. 7: 311–322.

Hirano, T., R. Kobayashi, and M. Hirano, 1997 Condensins, chromosome condensation protein complexes containing XCAP-C, XCAP-E and a Xenopus homolog of the Drosophila Barren protein. Cell 89: 511–521.

Jackson, D. A., 2010 Spatial epigenetics: linking nuclear structure and function in higher eukaryotes. Essays Biochem. 48: 25–43.

Januschke, J., L. Gervais, S. Dass, J. A. Kaltschmidt, H. Lopez-Schier *et al.*, 2002 Polar transport in the Drosophila oocyte requires Dynein and Kinesin I cooperation. Curr. Biol. 12: 1971–1981.

Jha, S., and A. Dutta, 2009 RVB1/RVB2: running rings around molecular biology. Mol. Cell 34: 521–533.

Joshi, A. A., and K. Struhl, 2005 Eaf3 chromodomain interaction with methylated H3–K36 links histone deacetylation to Pol II elongation. Mol. Cell 20: 971–978.

Joyce, E. F., B. R. Williams, T. Xie, and C. T. Wu, 2012 Identification of genes that promote or antagonize somatic homolog pairing using a high-throughput FISH-based screen. PLoS Genet. 8: e1002667.

Kennison, J. A., and J. W. Southworth, 2002 Transvection in Drosophila. Adv. Genet. 46: 399–420.

Kusch, T., L. Florens, W. H. Macdonald, S. K. Swanson, R. L. Glaser *et al.*, 2004 Acetylation by Tip60 is required for selective histone variant exchange at DNA lesions. Science 306: 2084–2087.

Leung, J. K., N. Berube, S. Venable, S. Ahmed, N. Timchenko *et al.*, 2001 MRG15 activates the B-myb promoter through formation of a nuclear complex with the retinoblastoma protein and the novel protein PAM14. J. Biol. Chem. 276: 39171–39178.

Lewis, E. B., 1954 The theory and application of a new method of detecting chromosomal rearrangements in *Drosophila melanogaster*. Am. Nat. 88: 225–239.

Lieberman-Aiden, E., N. L. van Berkum, L. Williams, M. Imakaev, T. Ragoczy *et al.*, 2009 Comprehensive mapping of long-range interactions reveals folding principles of the human genome. Science 326: 289–293.

Lomvardas, S., G. Barnea, D. J. Pisapia, M. Mendelsohn, J. Kirkland *et al.*, 2006 Interchromosomal interactions and olfactory receptor choice. Cell 126: 403–413.

Longworth, M. S., A. Herr, J. Y. Ji, and N. J. Dyson, 2008 RBF1 promotes chromatin condensation through a conserved interaction with the Condensin II protein dCAP-D3. Genes Dev. 22: 1011–1024.

Luco, R. F., Q. Pan, K. Tominaga, B. J. Blencowe, O. M. Pereira-Smith *et al.*, 2010 Regulation of alternative splicing by histone modifications. Science 327: 996–1000.

Luco, R. F., M. Allo, I. E. Schor, A. R. Kornblihtt, and T. Misteli, 2011 Epigenetics in alternative pre-mRNA splicing. Cell 144: 16–26.

Manning, A. L., M. S. Longworth, and N. J. Dyson, 2010 Loss of pRB causes centromere dysfunction and chromosomal instability. Genes Dev. 24: 1364–1376.

McManus, C. J., M. O. Duff, J. Eipper-Mains, and B. R. Graveley, 2010 Global analysis of trans-splicing in Drosophila. Proc. Natl. Acad. Sci. USA 107: 12975–12979.

Moore, S. A., Y. Ferhatoglu, Y. Jia, R. A. Al-Jiab, and M. J. Scott, 2010 Structural and biochemical studies on the chromo-barrel domain of male specific lethal 3 (MSL3) reveal a binding preference for mono- or dimethyllysine 20 on histone H4. J. Biol. Chem. 285: 40879–40890.

Morris, J. R., J. Chen, S. T. Filandrinos, R. C. Dunn, R. Fisk *et al.*, 1999 An analysis of transvection at the yellow locus of *Drosophila melanogaster*. Genetics 151: 633–651.

Ono, T., A. Losada, M. Hirano, M. P. Myers, A. F. Neuwald *et al.*, 2003 Differential contributions of condensin I and condensin II to mitotic chromosome architecture in vertebrate cells. Cell 115: 109–121.

Qi, D., H. Jin, T. Lilja, and M. Mannervik, 2006 Drosophila Reptin and other TIP60 complex components promote generation of silent chromatin. Genetics 174: 241–251.

Rajapakse, I., and M. Groudine, 2011 On emerging nuclear order. J. Cell Biol. 192: 711–721.

Rajapakse, I., M. D. Perlman, D. Scalzo, C. Kooperberg, M. Groudine *et al.*, 2009 The emergence of lineage-specific chromosomal topologies from coordinate gene regulation. Proc. Natl. Acad. Sci. USA 106: 6679–6684.

Rawlings, J. S., M. Gatzka, P. G. Thomas, and J. N. Ihle, 2011 Chromatin condensation via the condensin II complex is required for peripheral T-cell quiescence. EMBO J. 30: 263–276.

Roix, J. J., P. G. McQueen, P. J. Munson, L. A. Parada, and T. Misteli, 2003 Spatial proximity of translocation-prone gene loci in human lymphomas. Nat. Genet. 34: 287–291.

Rothbauer, U., K. Zolghadr, S. Muyldermans, A. Schepers, M. C. Cardoso *et al.*, 2008 A versatile nanotrap for biochemical and functional studies with fluorescent fusion proteins. Mol. Cell. Proteomics 7: 282–289.

Sanyal, A., D. Bau, M. A. Marti-Renom, and J. Dekker, 2011 Chromatin globules: A common motif of higher order chromosome structure? Curr. Opin. Cell Biol. 23: 325–331.

Shintomi, K., and T. Hirano, 2011 The relative ratio of condensin I to II determines chromosome shapes. Genes Dev. 25: 1464–1469.

Soutoglou, E., J. F. Dorn, K. Sengupta, M. Jasin, A. Nussenzweig *et al.*, 2007 Positional stability of single double-strand breaks in mammalian cells. Nat. Cell Biol. 9: 675–682.

Spilianakis, C. G., M. D. Lalioti, T. Town, G. R. Lee, and R. A. Flavell, 2005 Interchromosomal associations between alternatively expressed loci. Nature 435: 637–645.

Sutherland, H., and W. A. Bickmore, 2009 Transcription factories: Gene expression in unions? Nat. Rev. Genet. 10: 457–466.

Takizawa, T., P. R. Gudla, L. Guo, S. Lockett, and T. Misteli, 2008 Allele-specific nuclear positioning of the monoallelically expressed astrocyte marker GFAP. Genes Dev. 22: 489–498.

Vazquez, J., A. S. Belmont, and J. W. Sedat, 2002 The dynamics of homologous chromosome pairing during male Drosophila meiosis. Curr. Biol. 12: 1473–1483.

Wood, A. J., A. F. Severson, and B. J. Meyer, 2010 Condensin and cohesin complexity: the expanding repertoire of functions. Nat. Rev. Genet. 11: 391–404.

Wu, C. T., and J. R. Morris, 1999 Transvection and other homology effects. Curr. Opin. Genet. Dev. 9: 237–246.

Wysocka, J., P. T. Reilly, and W. Herr, 2001 Loss of HCF-1-chromatin association precedes temperature-induced growth arrest of tsBN67 cells. Mol. Cell. Biol. 21: 3820–3829.

Xie, T., R. Graveline, G. S. Kumar, Y. Zhang, A. Krishnan *et al.*, 2012 Structural basis for molecular interactions involving MRG domains: implications in chromatin biology. Structure 20: 151–160.

Xing, H., D. C. Wilkerson, C. N. Mayhew, E. J. Lubert, H. S. Skaggs *et al.*, 2005 Mechanism of hsp70i gene bookmarking. Science 307: 421–423.

Xing, H., N. L. Vanderford, and K. D. Sarge, 2008 The TBP-PP2A mitotic complex bookmarks genes by preventing condensin action. Nat. Cell Biol. 10: 1318–1323.

Xu, Y., C. G. Leung, D. C. Lee, B. K. Kennedy, and J. D. Crispino, 2006 MTB, the murine homolog of condensin II subunit CAP-G2, represses transcription and promotes erythroid cell differentiation. Leukemia 20: 1261–1269.

Yeong, F. M., H. Hombauer, K. S. Wendt, T. Hirota, I. Mudrak *et al.*, 2003 Identification of a subunit of a novel Kleisin-beta/SMC complex as a potential substrate of protein phosphatase 2A. Curr. Biol. 13: 2058–2064.

Zaidi, S. K., D. W. Young, M. Montecino, J. B. Lian, J. L. Stein *et al.*, 2010 Architectural epigenetics: mitotic retention of mammalian transcriptional regulatory information. Mol. Cell. Biol. 30: 4758–4766.

Zhang, H., Y. Li, J. Yang, K. Tominaga, O. M. Pereira-Smith *et al.*, 2010 Conditional inactivation of MRG15 gene function limits survival during larval and adult stages of Drosophila melanogaster. Exp. Gerontol. 45: 825–833.

Zhang, P., J. Du, B. Sun, X. Dong, G. Xu *et al.*, 2006 Structure of human MRG15 chromo domain and its binding to Lys36-methylated histone H3. Nucleic Acids Res. 34: 6621–6628.

Communicating editor: J. Sekelsky

GENETICS

Supporting Information
http://www.genetics.org/lookup/suppl/doi:10.1534/genetics.113.153544/-/DC1

Maintenance of Interphase Chromosome Compaction and Homolog Pairing in *Drosophila* Is Regulated by the Condensin Cap-H2 and Its Partner Mrg15

Helen F. Smith, Meredith A. Roberts, Huy Q. Nguyen, Maureen Peterson, Tom A. Hartl, Xiao-Jun Wang, Joseph E. Klebba, Gregory C. Rogers, and Giovanni Bosco

Copyright © 2013 by the Genetics Society of America
DOI: 10.1534/genetics.113.153544

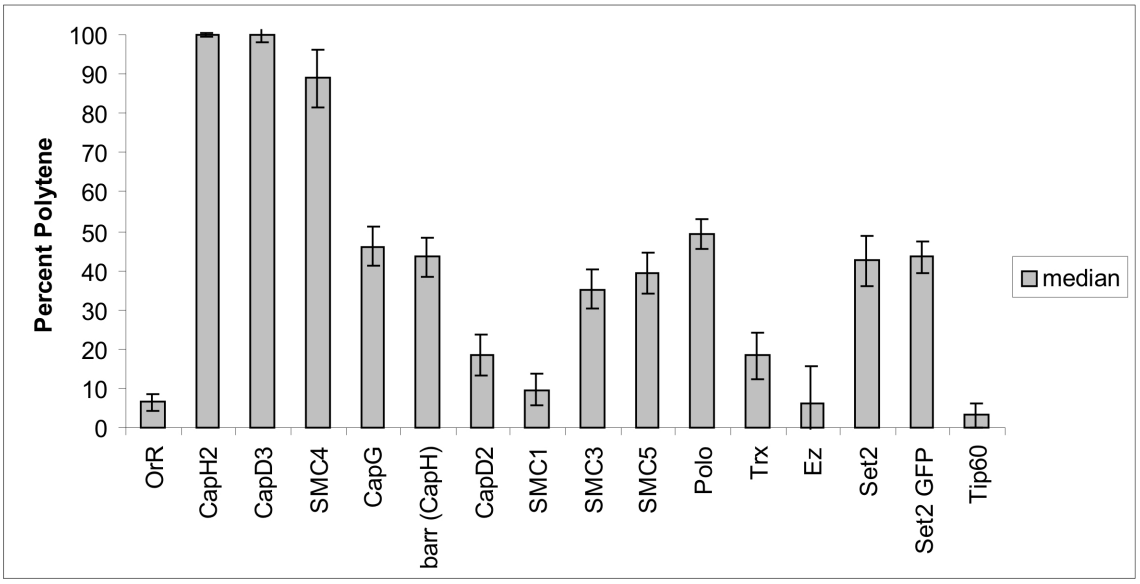

Figure S1 RNAi suppression in salivary glands overexpressing Cap-H2. The graph represents the median value for the various Vienna RNAi lines crossed into the "spots" genotype (LacO 60F, hs83>LacI-GFP; Hsp70>Gal4, *Cap-H2*^{EY09979}), except for the first one, OrR, which is not a RNAi line. The percent polytene was determined by DAPI staining for identification of polytene bands present under 40x magnification. Error bars are shown. See supplemental Table S2 for complete genotype description, number of nuclei and p-values.

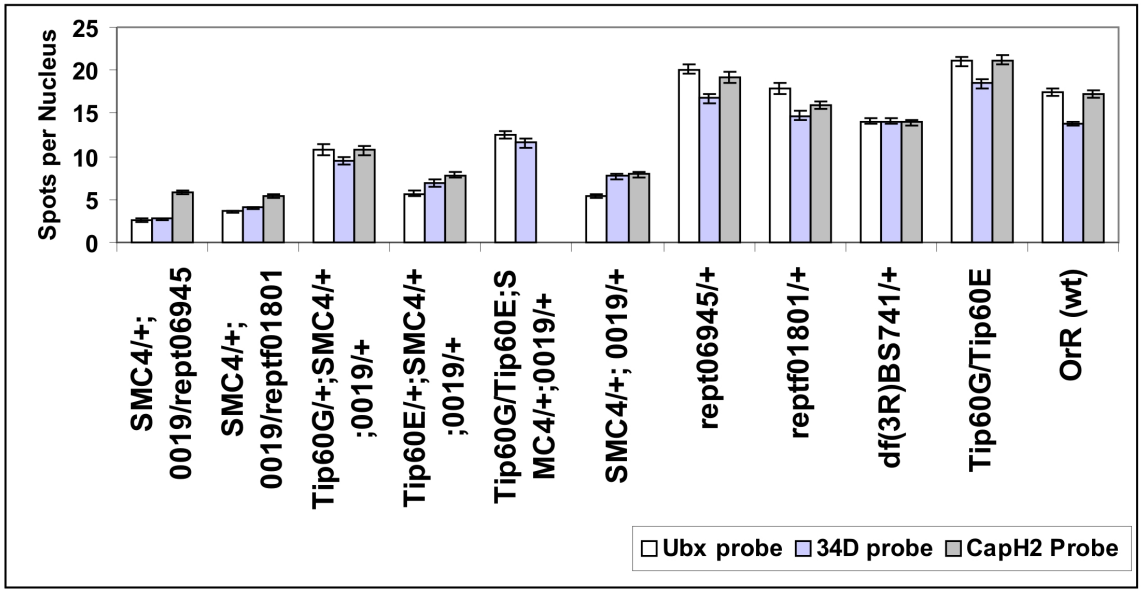

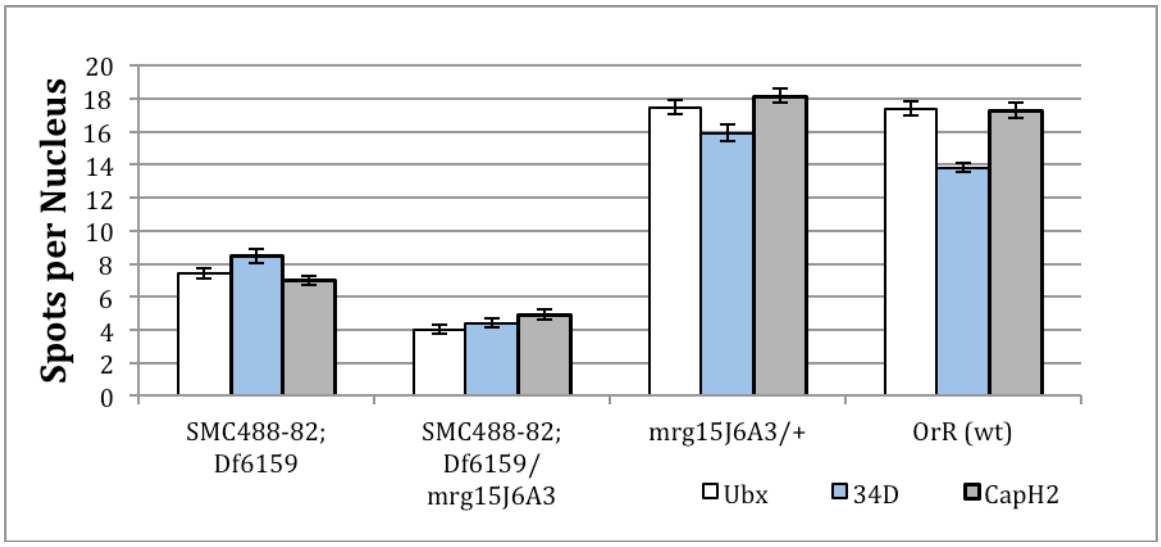

FigureS2 Condensin II interactors in the ovarian nurse cells. The graphs shows the number of FISH spots per nucleus in stage 6/7 eggchambers for each of the genotypes listed on the x-axis. The white bar represents the Ubx genomic region FISH probe, light blue is the 34D genomic region FISH probe, and grey is the Cap-H2 genomic region FISH probe. 0019 denotes the allelic designations for *Cap-H2*$^{Z3\text{-}0019}$. The *SMC4* allele used in the top graph is *Smc4*^{k08819} and for the bottom graph *Smc4*$^{88\text{-}82}$. The deficiency uncovering the *Mrg15* locus is Df(3R)BSC741. The deficiency uncovering the Cap-H2 locus is Df(3R)Exel6159 abbreviated as "Df6159". The list of complete genotypes is found in supplemental Table S2 along with the number of nurse cells for each probe and p-values.

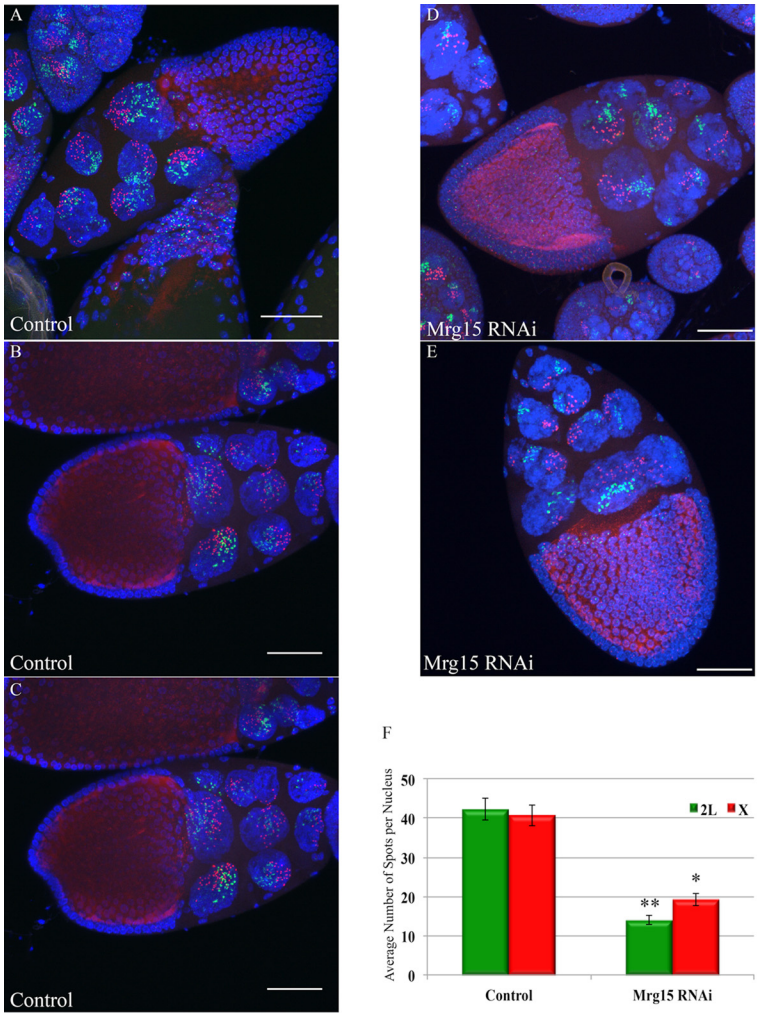

FigureS3 Germline specific RNAi depletion of Mrg15 leads to polytene unpairing defects. DNA FISH probes to chromosome 2L (green spots) and X-chromosome (red spots) in representative stage 10 eggchambers (DAPI in blue). Note that the unpairing defect was too severe in earlier stages and thus made quantitation of individual spots difficult. Panels A-C are control *Matα4-GAL-VP16* and panels D-E are *Matα4-GAL-VP16, Mrg15-TRiP-GL00128* RNAi depleted tissues (see methods). Panel F, number of FISH spots per nucleus were counted manually in 3D images for 3 different stage 10 eggchambers, and average number of spots is shown with standard error of the mean (two-tailed T-test, assuming unequal variance was calculated using MS Excel $*p<10^{-6}$; $**p<10^{-8}$). For 2L-probes n=17 (control) and n=18 (Mrg15 RNAi) nuclei. For X-probes n=16 (control) and n=16 (Mrg15 RNAi) nuclei. Images acquired with a Nikon laser scanning confocal with a 40x oil immersion lens (see methods), and 2D projections of a limited number of z-optical sections are shown. Scale bars are 50µm in each panel. See Figure 6 of main text for higher magnification images of individual stage 10 nuclei with FISH signals.

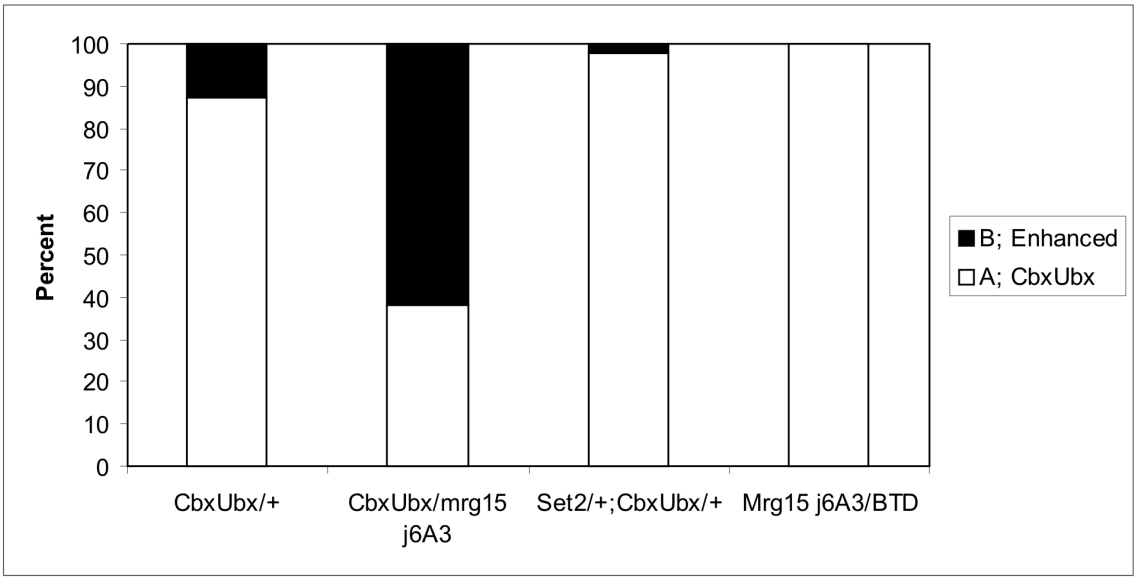

FigureS4 Transvection in *Mrg15*. Wings from the genotypes shown on x-axis were scored as either typical $Ubx^{Cbx\text{-}1}Ubx^{1}$ (class A, white bar) or enhanced (class B, black bar). Note that "typical" class A wings are not wild type and instead have a moderate abnormal morphology as a result of the transvecting $Ubx^{Cbx\text{-}1}$ allele. See Figure 7 of main text for images of typical wings. For simplicity, $Ubx^{Cbx\text{-}1}Ubx^{1}$ is denoted above as "CbxUbx". The data presented in this Figure S4 for $Mrg15^{j6A3}$ was derived independently of the data in Figure 7 of the main text. As an additional control, the $Set^{1}/+$ mutation has no significant effect on this transvection system. The last genotype includes the bithorax transvection disruptor (BTD), which is a rearrangement of the $Ubx^{Cbx\text{-}1}Ubx^{1}$ chromosome. N>61 for all genotypes. P-values using chi-squared relative to $Ubx^{Cbx\text{-}1}Ubx^{1}$/++ enhanced class: $Mrg15^{j6A3}$ p<0.001, $Set2^{1}$ p=0.74, $Mrg15^{j6A3}$/BTD *p<0.005*. The $Set2^{1}$ mutation has no significant affect on transvection in this assay and serves as a negative control. Note that since only one *Set2* mutant allele was tested we cannot exclude the possibility that other *Set2* mutations may modify transvecting loci.

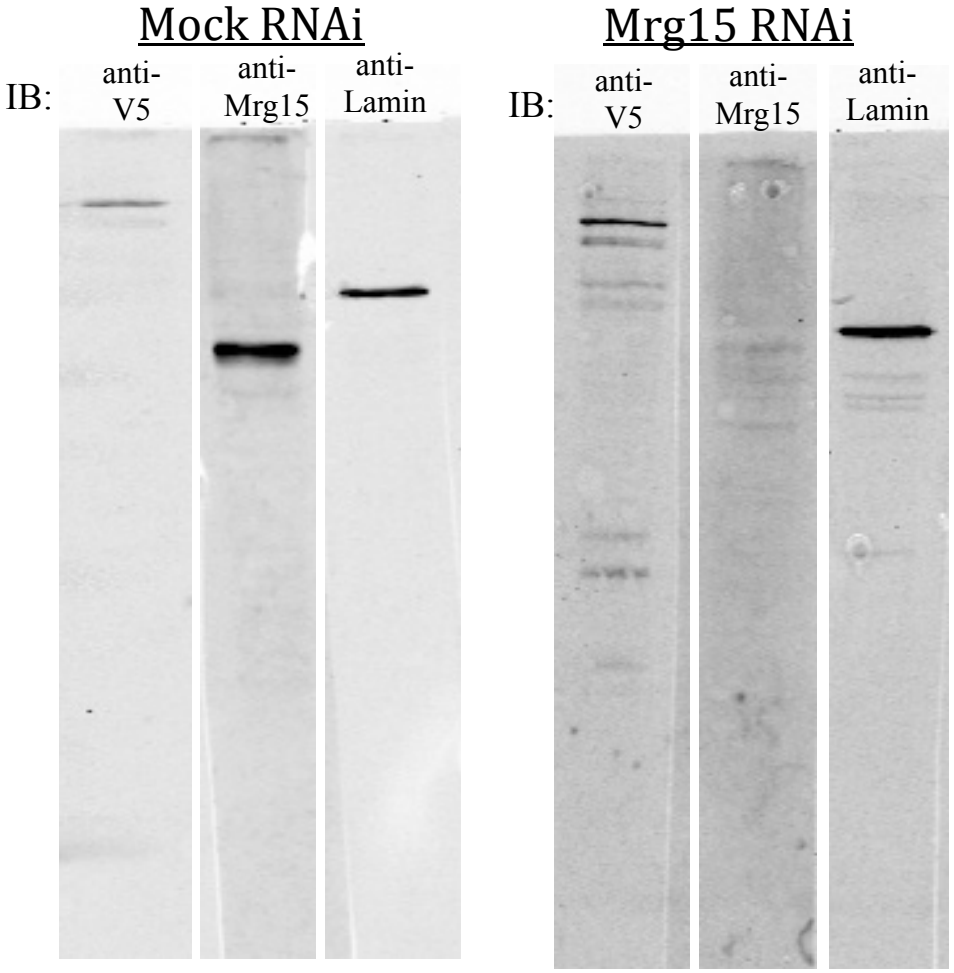

Figure S5 RNAi depletion of Mrg15 protein in S2 cultured cells. Cells were transfected with pMT-Cap-H2-V5 (or Cap-H2-EGFP; only V5 shown here) and were treated with double stranded RNA to pBlueScript SK (control Mock RNAi) or to Mrg15. Whole cell lysates were used for immunoblots (IB) with anti-V5, anti-Mrg15 or anti-Lamin (Dm0, Lamin B). Approximately >75% of Mrg15 protein was observed to be consistently depleted over four biological replicates. Protein depletion was determined from immunoblots exposed to film, scanned and quantitated using ImageJ. Lamin Dm0 bands in the linear range were used as loading controls.

Table S1 List of yeast two-hybrid interactors. The list of clones recovered from the yeast two-hybrid screen. The insert size in base pairs was estimated from PCR products (see main text for methods). The gene descriptor and CG numbers are as given from www.flybase.org based on blast search results from sequenced clones.

clone #	size of insert	gene descriptor	CG-identifier
1CH2-64-1	1000	unknown (eIF-3-p25 domain, Eukaryotic translation initiation factor 3 subunit 12)	CG10306
1CH2-39	500	unknown (methyltransferase-like protein)	CG10584
1CH2-65	400	Programmed cell death 4 ortholog (Pdcd4)	CG10990
1CH2-83-3	200	RpS12	CG11271
1CH2-76-3	250	RpS12	CG11271
1CH2-4	1100	Mitochondrial ribosomal protein S22	CG12261
1CH2-21	200	Pleckstrin-like protein (PH domain-containing)	CG12393
1CH2-32	300	Ribosomal protein L8	CG1263
1CH2-54-1	900	beta-site APP-cleaving enzyme	CG13095
1CH2-7-1	1000	yellow-g2, yellow protein (contain MRJP domain)	CG13804
1CH2-68	900	Chorion protein a at 7F	CG33962
1CH2-83-1	900	lethal (3) 03670 (unknown function)	CG1715
1CH2-51-4	180	RpL5	CG17489
1CH2-14	360	Glutathione S transferase E6	CG17530
1CH2-1	360	Ribosomal protein L31	CG1821
1CH2-28	400	Ribosomal protein S7	CG1883
1CH2-63-1	300	RpS7	CG1883
1CH2-61	800	Translation elongation factor 2b (Ef2b)	CG2238
1CH2-77	550	Translation elongation factor 2b	CG2238
1CH2-2	1000	Yolk protein 1	CG2985
1CH2-73	1350	Yolk protein 1 (Yp1)	CG2985
1CH2-78	120	Yolk protein 1 (Yp1) (same as 1CH2-73)	CG2985
1CH2-45-1	950	Yolk protein 1	CG2985
1CH2-67-1	880	Yolk protein 1	CG2985
1CH2-58	1300	Yolk protein 1	CG2985
1CH2-72-1	900	Yolk protein 1	CG2985
1CH2-45-2	300	RpL41	CG30425
1CH2-72-3	200	RpL41	CG30425
1CH2-64-2	800	14-3-3 epsilon (PAR5, EK3-5, 14-3-3)	CG31196
1CH2-7-2	230	RpL12	CG3195
1CH2-17	360	Pyroglutamyl-peptidase I	CG32147
1CH2-80	250	singed, structural constituent of cytoskeleton	CG32858
1CH2-79-1	780	26S proteasome regulatory complex subunit p42D (Rpt4)	CG3455
1CH2-53	900	unknown (Xylutokinase activity, FGGY-N and FGGY -C domains)	CG3534
1CH2-60	900	bellwether (blw), mitochondrial ATP synthase subunit alpha precursor	CG3612
1CH2-74	700	Mitochondrial ATP synthase alpha subunit	CG3612
1CH2-34	600	Ribosomal protein L23	CG3661
1CH2-19	450	Eukaryotic initiation factor 4E (eIF-4E)	CG4035
1CH2-54-2	500	RpS16	CG4046
1CH2-26	1000	Unknown	CG40460
1CH2-51-1	1150	Unknown	CG40460
1CH2-18	350	Ribosomal protein L35 RpL35	CG4111
1CH2-69	300	Eukaryotic initiation factor 2 (eIF-2 beta)	CG4153
1CH2-59	410	Heat shock protein hsp26	CG4183

1CH2-44	200	SUMO/Ubiquitin-like protein SMT3	CG4494
1CH2-8-2	280	RpLP2	CG4918
1CH2-67-2	600	RpS2	CG5920
1CH2-37	650	Vacuolar proton-motive ATPase subunit G VHA13	CG6213
1CH2-41	800	MRG15	CG6363
1CH2-56	1400	MRG15	CG6363
1CH2-8-1	600	MRG15	CG6363
1CH2-52-2	390	Chorion protein 15	CG6519
1CH2-27	130	Chorion protein 19	CG6524
1CH2-66	530	Chorion protein 19	CG6524
1CH2-51-2	310	RpS25	CG6684
1CH2-51-3	280	RpS25	CG6684
1CH2-42	340	Unknown (Nuclear phosphoprotein p8)	CG6770
1CH2-72-2	500	Unknown (Nuclear phosphoprotein p8)	CG6770
1CH2-40-2	270	RpS3	CG6779
1CH2-5	600	Rack1, Receptor of activated protein kinase C1	CG7111
1CH2-15	400	Rack1	CG7111
1CH2-24	600	Rack1	CG7111
1CH2-49	600	Rack1	CG7111
1CH2-71	550	Rack1	CG7111
1CH2-40-1	450	Rack1	CG7111
1CH2-79-2	420	Rack1	CG7111
1CH2-36	300	Ribosomal protein LP0(RpLP0)	CG7490
1CH2-50	400	Ribosomal protein L11 (RpL11)	CG7726
1CH2-43	180	janus A (molecular function unknown, sex differentiation)	CG7933
1CH2-13	510	Unknown (WD40/YVTN repeat-like-containing domain)	CG8001
1CH2-23	350	Cystatin-like protein	CG8050
1CH2-84	160	Ribosomal protein L37A (RpL37A)	CG8527
1CH2-76-2	400	Jon25Biii (elastase activity, trypsin activity)	CG8871
1CH2-12	900	Glyceraldehyde 3 phosphate dehydrogenase 2	CG8893
1CH2-83-2	510	Vitelline membrane 26Aa (Vm26Aa)	CG9048
1CH2-11	360	palisade, TU-1 (vitelline membrane formation)	CG9050
1CH2-25	250	Vitelline membrane 34Ca (Vm34Ca)	CG9271
1CH2-30	900	Glutathione S-transferase-like protein	CG9362
1CH2-52-1	500	Glycoside hydrolase	CG9466
1CH2-76-1	500	Int6 (Translation initiation factor activity)	CG9677
1CH2-57	200	Unknown	CG9350
1CH2-29	60	empty vector	
1CH2-31	70	empty vector	
1CH2-81	40	empty vector	
1CH2-63-2	20	empty vector	

Table S2 Figure S1 supporting information. List of genes, stock numbers, number of glands (nuclei), and p-values for Figure S1. For stock number, BL=Bloomington, v=Vienna Drosophila RNAi Center. The p-value is a two-tailed student t-test in Microsoft Excel and relative to the Oregon-R (OrR-S).

Gene	Stock #	# glands (nuclei)	p-value to OrR
OrR-S	BL4269	29 (1876)	NA
Cap-H2	v24905	15 (1068)	1.14x 10-28
Cap-D3	v9402	11 (584)	1.91x 10-23
SMC4	v10937	14 (882)	8.02x 10-14
Cap-G	v40047	26 (1634)	4.20x 10-11
Cap-H	v26760	23 (1303)	1.55x 10-7
Cap-D2	v33424	22 (1209)	1.01x 10-4
SMC1	v6532	23 (1460)	1.12x 10-2
SMC3	v39205	30 (1654)	3.42x 10-7
SMC5	v38969	37 (1952)	1.67x 10-6
Polo	v20177	27 (1429)	8.16x 10-11
Trithorax	v37715	6 (369)	4.58x 10-5
E(z)	v27646	5 (249)	0.27
Set2	v30707	33 (1467)	1.54x 10-12
Set2-GFP	BL24108	11 (532)	1.21x 10-9
Tip60	v22233	11 (554)	0.931

Table S3 Figure S2 supporting information. "Abbr" denotes abbreviation of genotype used in supplemental Figure S2. List of genotypes, number (n) of nurse cells for each of the three FISH probes, and p-values for supplemental Figure S2. The *Smc4* allele is $SMC4^{k08819}$ and the *Cap-H2* allele is $Cap\text{-}H2^{Z3\text{-}0019}$. The p-value is a two-tailed student T-test in Microsoft Excel and relative to the OrR-S. "nd" denotes not done.

Abbr.	Genotype	T-test to Genotype	Ubx FISH	34D FISH	Cap-H2 FISH	n of Ubx	n of 34D	n of Cap-H2
	SMC4/+;Cap-H2/reptin^P{PZ}06945	SMC4/+;Cap-H2/+	2.07E-15	1.88E-20	3.10E-07	125	37	115
	SMC4/+;Cap-H2/reptin^Pbac{WH}f01801		9.99E-08	2.66E-14	2.63E-08	77	59	63
	SMC4/+;Cap-H2/Mrg15^j6A3		1.58E-12	3.72E-08	3.92E-13	124	19	83
Tip60G	Tip60^P{Mae-UAS.6.11}GG01739/+; SMC4/+;Cap-H2/+		2.13E-12	5.21E-03	1.80E-06	75	49	79
Tip60E	Tip60^Pbac{RB}e02395/+;SMC4/+;Cap-H2/+		4.01E-01	1.63E-01	8.37E-01	89	55	92
	Tip60G/Tip60E; SMC4/+; Cap-H2/+		7.01E-28	2.43E-09	nd	89	81	nd
	SMC4/+;Cap-H2/+	OrR-S	9.36E-53	3.93E-26	1.34E-32	59	61	74
	reptin^P{PZ}06945/+		1.64E-04	2.13E-05	1.28E-02	86	72	63
	reptin^Pbac{WH}f01801/+		4.76E-01	1.64E-01	7.49E-02	63	48	68
Mrg15Df	Df(3R)BSC741/+		2.06E-08	5.51E-01	5.88E-08	63	59	58
	Tip60G/Tip60E		3.49E-07	2.11E-10	1.46E-08	79	57	86
wt	OrR-S					101	86	82

Table S4 Figure 10 supporting information. Supporting data for Figure 10 and pair-wise three-dimensional distance of FISH probes in cultured Kc_{167} cells. Treatment for RNAi depletion or Cap-H2 overexpression (OE), average distance in micrometers (μm), number of nuclei measured (N), standard error of the mean (SEM) and two-tailed, unequal variance T-test p-values, versus (vs) control RNAi samples, are shown. X-chromosome probes X1 is at ~9.4Mb, X2 is at ~7.35Mb and X3 is at ~5.8Mb). Second-Chromosome probes on the left arm (2L) are at ~10.3Mb and ~8.3Mb. All coordinates are taken from the *Drosophila melanogaster* genome version BDGP R5/dm3 (2006) using the UC Santa Cruz genome browser.

Treatment	Average Distance (μm)	N (nuclei)	SEM	P-value vs Control
X1 vs X2 (~2.05Mb apart)				
Control RNAi	0.96	66	0.04	
Cap-H2 RNAi	1.17	63	0.05	0.001
Mrg15 RNAi	1.14	54	0.06	0.009
Cap-H2, Mrg15 (double) RNAi	1.19	27	0.09	0.020
Cap-H2 (OE)	0.71	23	0.05	<0.001
X1 vs X3 (~3.6Mb Apart)				
Control RNAi	1.08	53	0.05	
Cap-H2 RNAi	1.26	58	0.06	0.019
Mrg15 RNAi	1.24	49	0.06	0.028
Cap-H2, Mrg15 (double) RNAi	1.49	39	0.09	<0.001
Cap-H2 (OE)	0.67	22	0.06	<0.001
2L (~2Mb apart)				
Control RNAi	0.81	46	0.04	
Cap-H2 RNAi	1.00	49	0.05	0.005
Mrg15 RNAi	1.06	30	0.06	0.002
Cap-H2, Mrg15 (double) RNAi	1.32	35	0.09	<0.001
Cap-H2 (OE)	0.65	19	0.05	0.002